

Observations in the vicinity of substorm onset: Implications for the substorm process

R. D. Elphinstone,¹ D. J. Hearn,¹ L. L. Cogger,¹ J. S. Murphree,¹ H. Singer,²
 V. Sergeev,³ K. Mursula,⁴ D. M. Klumpar,⁵ G. D. Reeves,⁶ M. Johnson,¹ S. Ohtani,⁷
 T. A. Potemra,⁷ I. Sandahl,⁸ E. Nielsen,⁹ M. Persson,¹⁰ H. Opgenoorth,¹⁰
 P. T. Newell,⁷ and Y. I. Feldstein¹¹

Abstract. Multi-instrument data sets from the ground and satellites at both low and high altitude have provided new results concerning substorm onset and its source region in the magnetosphere. Twenty-six out of 37 substorm onset events showed evidence of azimuthally spaced auroral forms (AAFs) prior to the explosive poleward motion associated with optical substorm onset. The azimuthal wavelengths associated with these onsets were found to range between 132 and 583 km with a mean value of 307 ± 115 km. The occurrence rate increased with decreasing wavelength down to a cutoff wavelength near 130 km. AAFs can span 8 hours of local time prior to onset and generally propagate eastward in the morning sector. Onset itself is, however, more localized spanning only about 1 hour local time. The average location of the peak intensity for 80 onsets was 65.9 ± 3.5 CGMlat, 22.9 ± 1.2 Mlt, whereas the average location of the AAF onsets was at 63.8 ± 3.3 CGMlat, 22.9 ± 1.1 Mlt. AAF onsets occur during time periods when the solar wind pressure is relatively high. These low-latitude wavelike onsets appear as precursors in the form of long-period magnetic pulsations (Pc 5 band) and frequently occur on the equatorward portion of the double oval distribution. AAFs brighten in conjunction with substorm onset leading to the conclusion that they are a growth phase activity causally related to substorm onset. Precursor activity associated with these AAFs is also seen near geosynchronous orbit altitude and examples show the relationship between the various instrumental definitions of substorm onset. The implied mode number (30 to 135) derived from this work is inconsistent with cavity mode resonances but is consistent with a modified flute/ballooning instability which requires azimuthal pressure gradients. It is suggested that this instability exists in growth phase but that an additional factor exists in the premidnight sector which results in an explosive onset. The extended source region and the distance to the open-closed field line region constrain reconnection theory and local mechanisms for substorm onset. It is demonstrated that multiple onset substorms can exist for which localized dipolarizations and the Pi 2 occur simultaneously with tail stretching existing elsewhere. Further, the tail can be less stretched at geosynchronous orbit during the optical auroral onset than during the precursor pseudobreakups. These pseudobreakups can be initiated by auroral streamers which originate at the most poleward set of arc systems and drift to the more equatorward main UV oval. Observations are presented of these AAFs in conjunction with low- and high-altitude particle and magnetic field data. These place the activations at the interface between dipolar and taillike field lines probably near the peak in the cross-tail current. These onsets are put in the context of a new scenario for substorm morphology which employs individual modules which operate independently or couple together. This allows particular substorm events to be more accurately described and investigated.

1. Introduction

The study of optical auroral substorms has advanced considerably since the initial work by *Akasofu* [1964]. Their morphology has been investigated and relationships between the ionosphere and magnetosphere established. For example, the

¹ Department of Physics and Astronomy, University of Calgary, Calgary, Alberta, Canada.

Copyright 1995 by the American Geophysical Union.

Paper number 94JA02938.
 0148-0227/95/94JA-02938\$05.00

² National Oceanic and Atmospheric Administration, Boulder, Colorado.

³ Institute of Physics, University of St. Petersburg, St. Petersburg, Russia.

⁴ Department of Physics, University of Oulu, Oulu, Finland.

⁵ Space Science Laboratory, Lockheed Missiles and Space Company Inc., Palo Alto, California.

⁶ Los Alamos National Laboratory, Los Alamos, New Mexico.

⁷ Applied Physics Laboratory, Johns Hopkins University, Laurel, Maryland.

⁸ Swedish Institute for Space Physics, Kiruna, Sweden.

⁹ Max-Planck-Institute for Aeronomy, Lindau, Germany.

¹⁰ Swedish Institute for Space Physics, Uppsala, Sweden.

¹¹ IZMIRAN, Moscow Region, Troitsk, Russia.

existence of the growth phase was debated into the 1970s [McPherron, 1970; Starkov and Feldstein, 1971; Akasofu and Snyder, 1972; Feldstein, 1974]. It is now clear however that the growth phase does indeed occur and plays an important role in the substorm process [Pellinen and Heikkila, 1978; Kirkwood and Eliasson, 1990; Koskinen et al., 1992; Watanabe and Iijima, 1993]. It also appears that dayside auroral activity can accompany the growth of electrojets prior to substorm onset [Elphinstone et al., 1991a]. Akasofu [1964] divided the expansive phase of a substorm into different parts with the first stage lasting about 5 min. This coincided with the time before the poleward motion began. If the poleward motion lasted only a few minutes this was termed a pseudobreakup. Later the substorm onset [Akasofu and Kan, 1982, p. 1315] was "morphologically defined as the moment when an auroral arc brightens suddenly and begins to advance poleward." This "moment" can actually last more than 10 min and can be fundamental to understanding the cause of a substorm. One aspect of this paper will be to investigate this important time period in more detail using ultraviolet images acquired by the Canadian UV imager on board the Swedish Viking satellite.

Particular types of north-south auroral structures in the substorm bulge (called auroral streamers in what follows) which drift equatorward and eastward or westward depending on their local time were known by Akasofu [1964], but our understanding of their cause is still an active area of interest [Nakamura et al., 1993; Liu and Rostoker, 1993]. An arc system at the poleward edge of the aurora is now known to brighten toward the end of substorm expansive phase as the emissions within the bulge fade [Murphree and Elphinstone, 1988]. This can be accompanied by the formation of vortex streets and westward traveling spiral forms [Cogger and Elphinstone, 1992]. At the beginning of substorm recovery (defined by ground magnetometers and by the fading of the aurora within the bulge), the formation of a double westward electrojet begins (one associated with the main UV oval and the other with the more poleward system). It has been shown recently [Elphinstone et al., 1994] that this most poleward arc system is directly related to the velocity dispersed ion signature (VDIS) [Zelenyi et al., 1990] and develops separately from the auroral bulge itself. This together with what appears to be global mode oscillations of the magnetotail at this time supports the view that this arc system can be associated with the recovery of the plasma sheet. In this new description, the recovery begins with the formation of the double oval [Elphinstone and Hearn, 1992; Elphinstone et al., 1993a] which subdivides the wide active auroral oval [Feldstein and Starkov, 1967] into two distinctive regions. Either of these two regions can then further activate resulting in significant electrojet activity [Cogger and Elphinstone, 1992]. The history of an event therefore is fundamental to placing the event in a correct context in the larger-scale substorm process.

Originally, only the most equatorward arc brightening was considered to result in an intense substorm [Akasofu, 1966] and thus be an onset. Other arcs which brightened did not develop into full global substorms and so were called pseudobreakups [e.g., Akasofu, 1964; Ohtani et al., 1993; Nakamura et al., 1994]. McPherron [1979] summarized very well the more general concept of the magnetospheric substorm and described the evolution of multiple onset substorms [Pytte et al., 1976] and substorm sequences. Eastward propagating folds termed omega bands [Akasofu and Kimball, 1964; Opgenoorth et al., 1983] were known to exist during late expansive phase and substorm recovery. These form on the main UV oval (the equatorward

distribution) during times when the double oval exists and so originate deep within the closed field line region [Elphinstone et al., 1993a]. Pulsating auroras in the late evening and morning have also been investigated since the early 1960s [Royrvik and Davis, 1977; Thomas and Stenbaek-Nielsen, 1981]. Thus there have been many features of the substorm optical patterns which are relatively new additions to our understanding of the substorm process. The substorm schematic by Cogger and Elphinstone [1992] incorporates many of these new concepts and will be used as an underlying basis from which this paper will proceed.

Theories rely heavily on experiment to test their predictions. Over the years numerous models for the substorm process have been developed [see Fairfield, 1992, and references therein]. Reconnection theories have received the most attention and have evolved to account for new observations [e.g., Reeves et al., 1992]. Some of the theories involve boundary layer processes, including the thermal catastrophe theory which operates in the plasma sheet boundary layer [Goertz and Smith, 1989], and the theory suggested by Rostoker and Eastman [1987] which involves the Kelvin-Helmholtz instability in the low-latitude boundary layer. With evidence mounting that processes associated with onset can be found close to Earth [Kennel, 1992, and references therein], numerous models have been developed to account for this. These include the ballooning, flute, and/or interchange instability [Swift, 1967; Roux et al., 1991a; Ivanov et al., 1992], the cross-field current instability mechanism [Lui et al., 1991] and others such as those presented by Erickson and Heinemann [1992], and Haerendel [1992]. Other authors have included the effects of the ionosphere [Kan, 1993; Lysak, 1992], while still others have provided a synthesis which explains a wide range of observations [Lui, 1991].

All of these models make an attempt to explain the published observations concerning the substorm process. There are, however, a wide range of phenomena not covered in any detail as yet in the substorm literature. This paper will focus on the time period from the first intensification of an arc in the evening sector to the time when the bulge begins to form and move westward, eastward, and poleward. It will focus on a particular type of substorm onset in which intensifications periodically spaced in longitude appear before, during, and after substorm onset. We call these intensifications azimuthally spaced auroral forms (AAFs). Since the first evening intensification associated with a substorm can occur as long as 40 min before the actual explosive poleward motion, we will adopt the latter as a working definition of the time of optical substorm onset. The events leading up to this onset will be referred to as substorm precursors. An important aspect of this paper will be to show that the context and history of a given event can dramatically affect how that event develops and is interpreted.

The rest of this paper is divided into four main sections. The first deals with case by case examples of AAF onsets in order to illustrate the wide range of behavior which exists in the large-scale pattern. A number of examples were chosen to illustrate the variability and the effects of the activity level on how the substorm develops. It also shows how a number of different instruments view these events. This section draws on ground magnetometer data, radar, optical observations, and high- and low-altitude satellite observations of both particles and magnetic fields. A comparison is made between various definitions of "onset" in order to test for consistency. It is established that AAF activations are indeed substorm onsets as defined using

Table 1. Event Case Studies

Event, date	Instrumentation/Data Sets	Type of Prior Activity
October 3, 1986	ground magnetometers (20 s), <i>AL</i> , <i>AU</i> (1 min), <i>Dst</i> (1 hour), IMF (15 s), <i>SW*</i> (~1 min), Viking LBH UV image data (1 min), Pi 2/Pi B information, STARE radar (20 s)	contracted oval IMF B_z northward magnetosphere compressed
November 24, 1986	ground magnetometers (1 min), <i>AL</i> , <i>AU</i> , <i>Dst</i> , Viking LBH UV images, Pi 2/Pi 1B information	main phase of storm double oval configuration recovery phase of previous substorm
September 23, 1986	IMF, <i>SW</i> , <i>Dst</i> , Viking LBH UV images, Pi 2/Pi 1B information all-sky camera data (Laparskaya)	storm time double oval recovery phase of previous substorm
July 24, 1986	ground magnetometers, <i>AL</i> , <i>AU</i> , IMF, <i>S.W.</i> , <i>Dst</i> , Viking LBH UV images, CCE electron, ion fluxes and magnetic field, Pi 2/Pi 1B information, Tsyganenko mapping	magnetosphere compressed large growth phase after passage of coronal streamer
July 27, 1986	<i>Dst</i> , <i>AL</i> , <i>AU</i> , Viking LBH UV Images, DMSP F7 particle and magnetic field, Viking particle observations, Tsyganenko mapping, GOES 5 and 6 magnetic field, LANL geosynchronous sat. energetic particle fluxes	<i>AL</i> and <i>AU</i> indicate previously active time period multiple activation leading to double oval and AAF onset
April 16, 1986	IMF, <i>Dst</i> , <i>AL</i> , <i>AU</i> , Viking LBH UV images, DMSP F7 particle data, Tsyganenko mapping, GOES 5 and 6 and geomagnetic field, LANL geosynchronous sat. energetic particle fluxes, NOAA 6 energetic particle fluxes over onset locations	Multiple onset substorm during double oval event

* Solar Wind density and velocity.

other criteria. Table 1 briefly summarizes the geophysical conditions and the instrumentation used in this paper for the six subsections. Table 2 highlights the timing and the primary observations for each event. The reader should refer to these tables and the event summaries at the end of each subsection for an orientation concerning the events. Each subsection is further divided into parts which cover the geophysical conditions, the auroral and magnetic observations and finally data from both high- and low-altitude spacecraft.

Section 3 shows some statistics regarding these AAF onsets. In order to put these wavelike onsets into a more general context of the auroral substorm, section 4 shows how they fit into the overall description of optical auroral substorms. In this section a new proposal for the description of the auroral substorm is presented. Section 5 will discuss the relevance of the observations to substorm theories and attempt to discuss the pros and cons of different models based on the observations presented here.

2. Observations of Substorm Onset

2.1 Substorm During a Time of a Contracted Auroral Oval: Orbit 1232 (October 3, 1986)

This event was chosen to represent an AAF onset during a relatively quiet time when only the main UV oval was initially evident, and IMF B_z was northward. Auroral, magnetic and radar data in the vicinity of the AAFs help establish the timing of onset relative to the optical auroral development (see Tables 1 and 2).

Geophysical conditions. For this event the *Dst* index remained greater than -30 nT throughout the time interval of interest. Prior to onset the *Dst* increased to zero indicating that the magnetosphere was in a compressed state or that the magnetopause current was enhanced. During the substorm the *Dst* decreased indicating a net strengthening of the ring current during the event. The *AU* index (provisional in this and the following cases) remained less than 100 nT, and the *AL* index began to change at about 2030 UT and reached a peak value of about -250 nT during the event. The interplanetary magnetic field (IMF) and solar wind pressure are shown in Figure 1. The IMP 8 satellite was located at $x_{GSE} = 5.6 R_E$, $y = -36.1 R_E$, and $z = -17.2 R_E$. IMF B_z (GSM) was northward prior to 2028 UT except for brief southward excursions between 1920 and 1925 UT (to -0.8 nT) and between 1949 and 1951 UT (to -0.35 nT). It remained southward after 2028 UT. At 1911:21 UT, IMF B_x and B_y both changed sign to $B_y < 0$ and $B_x < 0$. Also at this time the solar wind pressure changed by a factor of 2 and the total IMF field decreased dramatically. After 2000 UT there was a gradual pressure increase by about 20% until the time of auroral brightening at 2020 UT (see below).

Auroral dynamics. The aurora shown in Plate 1 is an example of the aurora brightening during a time of IMF B_z northward about 1 hour after a significant solar wind pressure increase. The only way in which the B_z southward turning could have triggered this event would be if the discontinuity in the solar wind was oriented such that the magnetotail encountered the disturbance more than 9 min prior to IMP 8. There would also then have to be a delay to take into account propa-

Table 2. Timing of Principle Observations (hhmm - UT)

Event*	Geophysical Information	Auroral	Ground Magnetic/ Low Altitude Satellites	High-Altitude Satellites
1	IMF $B_z > 0$ until 2028 PP [†] at ~1911, 2000 1911 - IMF sector change $Dst > -30$ AL minimum ~-25 nT AU maximum < 100 nT	2019 arc brightens, eastward electrojet activates/AAFs form pulsations 2032 - onset 2049 new activation, onset and auroral streamer	1940 Pc 5 pulsations 2019 W [‡] , 2032 S [§] , 2049 W -Pi 2/Pi 1B 2038 - auroral streamer	none
2	1500 start of main phase AU < 200 nT 2010 - AL ~-360 nT 2044 - AL ~-1300 nT	2005 first AAFs/omega 2010 explosive onset - AAFs brighten with onset AAFs turn into spirals equatorward moving multiple arcs	2011 W, 2013 S, 2015 S, 2017 S, 2022 S, 2033 S, Pi 2/Pi 1B RH polarized Pc 5 pulsations east of onset; LH west of onset	none
3	large PP [†] previous day $Dst < -40$ nT for 12 hours previous AU > 200 nT AL changed from -100 to -700 nT IMF $B_z < 0$ after 2029 PP at 2034, 2046	2031, 2038 - prenoon aurora activates 2043 - 4 MLT activity 2047 - AAFs 2051 - SCW?/onset	2051 - Pi 2 onset LH polarized and frequency changes	none
4	1640-2106 - 5 PP [†] 2157 - IMF $B_z < 0$ 2221, 2232, 2245, 2252 - small PP [†] $Dst \sim 0$ for previous 2 days, 40 nT by 2000, and < 0 by 2300. 2220 - AU increases 2221, 2300 - AL decreases	2236 prenoon activations 2250 - AAFs form and drift east 2255 - AAFs intensify 2259 - intensification 2304 - explosive onset	2222 - ~2.2 mHz pulsations begin 2250 W ⁺ , 2254 S ⁺ , 2302, 2304 - Pi 1B pulsations	CCE 2254 - electron flux decrease and 35-mHz pulsations (0.35 keV) 2301-ion injection, electron spectrum hardens with no density change, DP [‡] 2304 - electron flux dropout, DP [‡] 2305 - flux recovers
5	$Dst \sim -20$ before onset and -40 after 0800 - AU increases 0830 - AL decreases 0930 - AL ~-1600 nT	0647 - dayside activity 0715 midnight activity 0730 activation and double oval 0747, 0811, 0820 - new activations 0829 - AAF onset	0736-0745, 0815-0820 DMSP-F7 overflights 0837 - Viking	LANL satellites electron injections 0643, 0716, 0730, 0746, 0835. proton injections 0716, 0752 GOES 5 and 6 0748 - Pi 2 0830 GOES 6 Pi 2, DP [‡] 0845 GOES 5 Pi 2, DP [‡]
6	Dst increasing AL, AU recovering until 0430 0311, 0335, 0354 - away sector azimuth angle decreases	0319, 0331, 0340, 0354, 0406, 0430 - activations on main UV oval 0319, 0331 - AAFs 0331 - auroral streamer associated	DMSP - 0326-0332 NOAA 6 0349-0357	LANL satellites 0319, 0331, 0340, flux enhancements/ drifting e ⁻ holes 0406, 0430 inject. GOES satellites 0319 weak DP [‡] 0340, 0406, 0430, stretching, DP [‡] Pi 2s

Event 1, October 3, 1986; 2, November 24, 1986; 3, September 23, 1986; 4, July 24, 1986; 5, July 27, 1986; 6, April 16, 1986.

† PP, pressure pulse.

‡ dipolarization.

§ S, strong pulsation; W, weak pulsation.

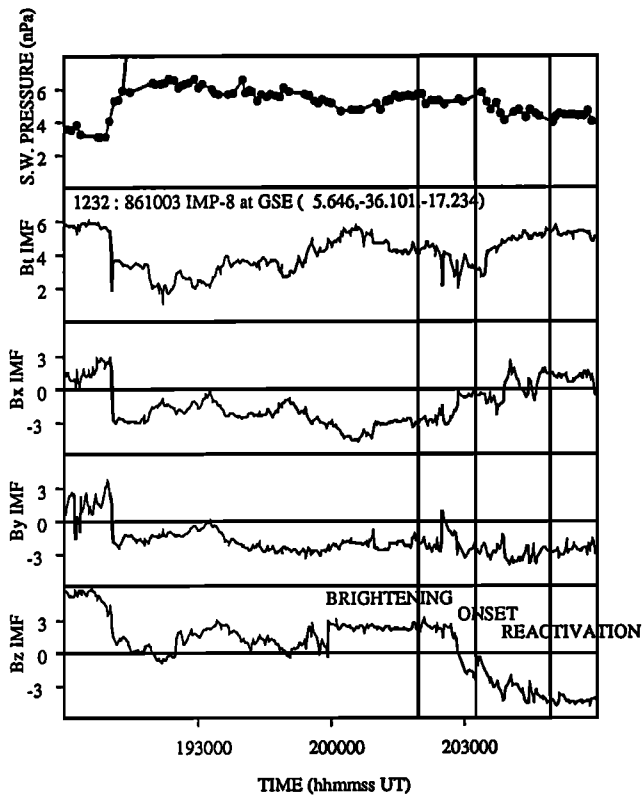


Figure 1. IMP 8 IMF solar wind data for the event shown in Plate 1.

gation times and any required growth phase (see *Sergeev et al.* [1986] for a discussion of this possibility). Although this could have occurred it seems simpler to assume that the event occurred during the period of IMF B_z northward and is an example of an onset of a main phase of a weak storm.

In Plate 1 and all others in this paper the UV aurora was recorded by the imager on board the Viking spacecraft in the wavelength range corresponding to the LBH bands between 1400 and 1800 Å (see *Anger et al.* [1987], *Murphree and Cogger* [1988], and *Cogger et al.* [1988] for a discussion of the instrumentation used). The images have been transformed from the view as seen from the satellite to a system in which each pixel element in the image represents a square of equal dimensions on each side (in Corrected Geomagnetic coordinates CGM80, as described by *Hearn et al.* [1993]).

At 2019:52 UT (second panel in top row) a localized arc enhancement took place. In three min this develops into multiple brightenings covering three hours local time (extending both to the west and to the east of the initial brightening). This first change could be considered to be an arc system appearing out of the background or could be the arc brightening sometimes used to define substorm onset. The difference between the two is simply a matter of degree. Observations from the STARE radar (see *Nielsen et al.* [1982] for an instrument description) showed that this first brightening coincided with an intensification of westward flow (eastward electrojet) just equatorward of the arc system. The radar is located near Abisko station in Plate 1 (the radar field of view is shown in the top row, second panel). By 2022 UT equally spaced in azimuth auroral forms (AAFs in what follows) have appeared.

The spatial scale of the AAFs will be expressed in terms of the corresponding mode number so that there is no need to deal

with the latitude at which they occur. The mode number is the number of the wavelengths which would fit into 2π rad. For this event, four "wavelengths" span three hours local time giving a mode number, m , of about 32. These were evaluated (in the original data) by simply counting the number of wavelengths in the MLT range over which they occurred. Although most of the features described in the text are clear in the plates there are instances where the reader may find it difficult to see the relevant forms. Since the color plates were designed with the entire event in mind the scale size of the AAF features in the plates were often not optimum and/or the color bar was chosen such that some of the features did not stand out. Also, the transformation from the satellite view to a polar coordinate system (which was important to aid the reader) can sometimes exaggerate regions of enhanced luminosity which were actually due to noise. The original data were used to evaluate the mode numbers in order to avoid these spurious effects. The mode numbers found in this observation section used measurements accurate only to about 0.5 MLT and so have an error of about ± 6 in terms of mode number. In a later section the spatial scale of the AAFs is found more precisely (see section 3).

Between 2019 and 2032 UT the region has brightened but no significant poleward motion has occurred. If onset is taken to be the start of poleward motion then this does not occur until between 2031:45 and 2032:45 UT or some 12 min after the initial arc appears. At this time the mode number of the AAFs in the ionosphere is slightly higher than previously, at about $m = 48$. AAFs continue to exist after this time until about 2037 UT. The growth of the disturbance and the motion of individual forms was westward premidnight (between 2019 and 2022 UT) and eastward postmidnight. Individual forms can be seen to drift eastward at 2 MLT between 2036 and 2038 UT.

Between 2038 and 2047 UT, a weak arc system appears and disappears to the east of the auroral surge. This type of arc system will be referred to as an "auroral streamer" in what follows. An auroral streamer is an auroral form which separates from the expanding bulge and drifts westward and equatorward. The substorm bulge fades after 15 min (2047:36 UT) and AAFs can be seen at this time to the west of the surge form. The bulge reintensifies with a westward traveling surge (WTS) and the formation of an auroral streamer between 2049:35 and 2054:32 UT. A weak double oval develops between 2042:32 and 2054 UT along with a polar arc system at the poleward edge of the diffuse oval. (The double oval is defined as two morphologically distinct auroral regions spanning a few hours of local time.)

The STARE radar backscatter signal fades by 2025 UT and then reintensifies at 2029 and 2032:40 UT. The intensification at 2032:40 UT was divided up into two separate convection shear flows at 16° and 22° Glon corresponding to the AAF seen at the west end of the newly forming substorm bulge. The sense of convection is consistent with upward field aligned current at the centers of the shear flows. Later between 2034 and 2036:20 UT poleward directed flow

Magnetometer observations. Lovozero registered Pi 2/Pi 1B activity clearly between 2032 and 2042 UT with other weak but clear bursts beginning at 2019 and 2049 UT (A. Yahnin, private communication, 1994). The pulsations at 2019, 2032, and 2049 UT correspond very well with the first arc brightening, the explosive poleward motion and with the reactivation of the bulge respectively. The weaker bursts at the time of the first intensification were only seen after a second examination of the

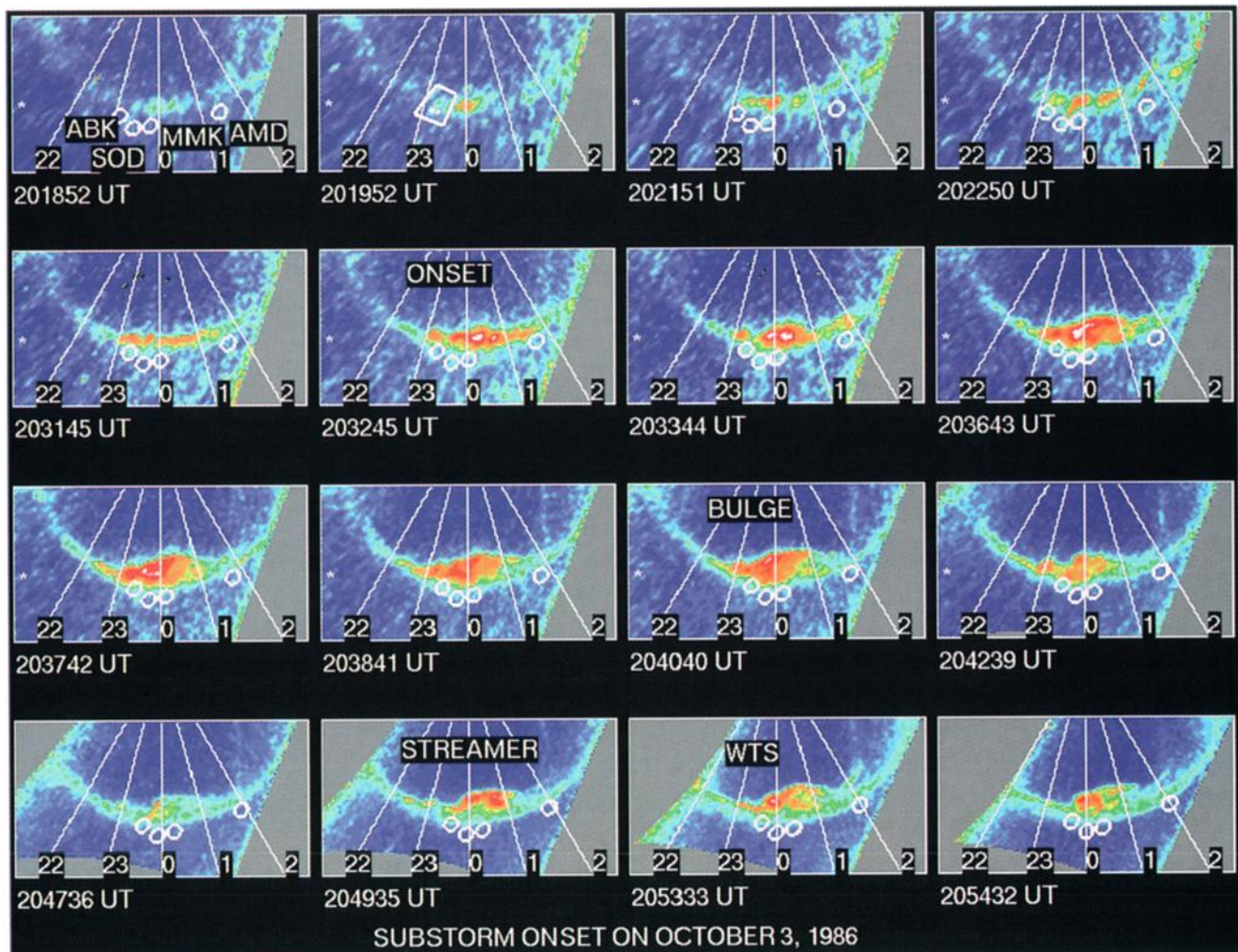


Plate 1. Viking auroral images from 2018:52 to 2054:32 UT on October 3, 1986. The local times plotted are 22, 23, 0, 1, and 2 MLT. The four ground stations are Abisko-ABK, Sodankyla-SOD, Loparskaya-MMK, and Amderma-AMD. Universal time in hhmmss are shown at the bottom of each panel. AAFs appear at 2022:50 UT (top right panel) some 10 min before substorm expansion begins. The second top panel shows the STARE radar field of view.

data took place when it was noticed that the arc brightening took place before the main P₁ 2 burst. Four magnetometer stations (Abisko-ABK, Sodankyla-SOD, Loparskaya-MMK, and Amderma-AMD) which lay equatorward of the onset region are marked by the large circles in Plate 1 (45° zenith angle field of views at 120 km altitude) and their *X* and *Y* magnetic field components are shown in Figure 2. Loparskaya station appears to be near the division between the eastward and westward electrojets just prior to 2020 UT. The intensification of an eastward current system equatorward and westward of the surge as implied by the magnetometer data is consistent with currents flowing around the surge. This current system is also seen in backscatter STARE observations. The intensifying westward electrojet at Amderma at 2032 UT is consistent with substorm current wedge formation at this magnetic local time.

To the west of onset long period pulsations at 3 mHz are seen which began about 1940 UT. The peak to peak amplitude was about 5–7 nT until 2016 UT at which time it increases to 21 nT. Just prior to onset the frequency at Abisko changed gradually to 2.2 mHz. The frequency information in this and other examples is based on a sonogram analysis. At onset a

number of higher frequencies appear. Similar results are seen at Sodankyla. To the east of onset, at Amderma, power in the low-frequency range was also seen beginning at about 1920 UT. Frequencies were first seen at less than 2 mHz. These changed to a higher frequency near 2.2 mHz just before onset. The timing associated with these pulsations (1920 and 1940 UT) is relatively consistent with the pressure increase which occurred in the solar wind at 1911 UT. The dominant frequencies after onset were at about 2.9 and 6 to 8 mHz. These oscillations were also evident in the *Y* component at Amderma. The time delays in the *X* component between Abisko, Sodankyla, and Amderma seen at 2022:50 UT in Figure 2 indicate an eastward motion of the pulsation activity near 2022 UT.

It is interesting to note that the drift to higher frequency occurred in conjunction with an equatorward motion of the auroras at this location and that this occurred prior to when the IMF turned southward. This motion can be seen by comparing the location of the aurora near 2 MLT with the Amderma field of view from 2022 to 2033 UT. A frequency drift from high to low frequency west of onset is consistent with a source moving outward in the magnetotail (i.e., to longer more stretched field

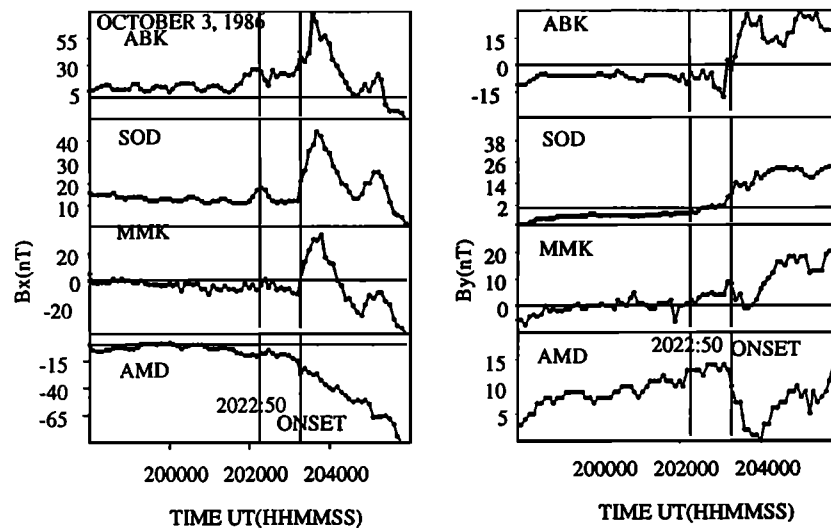


Figure 2. X and Y ground magnetic field data for ABK, SOD, MMK, and AMD for the event in Plate 1. The vertical lines show the times of the AAFs (2022:50 UT) and the poleward expansion (2032:45 UT). Long-period pulsations are evident.

lines) while the shift in the morning sector is consistent with an earthward movement of the source region.

Summary. A pressure change during IMF B_z northward appears to be associated with Pc 5 pulsation activity. An initial brightening in the midnight sector was preceded by these pulsations by about 40 to 50 min. It was not clear whether any solar wind disturbance was linked to this brightening although there was a small pressure enhancement just prior to it. The final explosive poleward motion and/or the later reintensification of the bulge may have been triggered by B_z turning south. The active region of the aurora at the time of the explosive poleward motion (2032 UT) was about 2 hours wide in local time (i.e., this was not a local or pointlike onset). The mode number increased towards the time of poleward motion. Pulsations which changed in frequency in the Pc 5 period range were seen prior to the poleward expansion and in association with the AAFs. The low-frequency component shifted to lower values west of onset and to higher values east of onset. The change in the east was consistent with an equatorward motion of the aurora in the east and may indicate an earthward or inner motion of the current sheet just prior to onset.

Before onset the mode number was about 32 and the frequency (f) about 2.2 mHz. Assuming these parameters are related to one another, an implied speed can be derived from them. The speed in km/s is about $2\pi R_E L 2.2/32000 = 2.8L$, where L is the L value at which the disturbance occurs and R_E is one Earth radius in km. If the source was between $L = 6$ and 10 then the associated magnetospheric speed was between 17 and 28 km/s. These speeds are comparable to the gradient drift speeds (V_d) of about 20 keV particles in the equatorial plane of a dipole field ($V_d = 0.016 L^2 E$ km/s, where L is the L value and E the energy of the particle in kiloelectron volts).

This event shows that there are clear cases where the time between the first brightening and the explosive poleward motion can last as long as 13 min. It also shows that there is an additional factor which triggers the onset after the formation of the AAFs. These precursors AAFs may be similar to the forms reported by Untiedt *et al.* [1978] prior to substorm expansion.

2.2 Substorm During the Main Phase of a Magnetic Storm: Orbit 1518 (November 24, 1986)

In contrast to the previous event, this case study involves a double auroral oval during active magnetic conditions. This event was chosen to illustrate that AAFs can coexist with omega bands, and to show how an onset can begin from the main UV oval and actively propagate poleward to the open-closed fieldline boundary. Subsequent activity can then begin from the more poleward region and move equatorward, influencing in turn the main UV oval.

Geophysical conditions. No IMF data were available for this event which began at about 2000 UT. The Dst showed that the main phase of a storm began at about 1500 UT, and by 2000 UT the Dst had become less than -60 nT. It further decreased to -80 nT by 2400 UT. The event therefore took place during a time of enhanced ring current. The AU index remained less than 200 nT. The AL index showed that the event in question took place during the recovery phase of a previous substorm. The index recovered from -1100 to -360 nT at which time (2010 UT) the new onset occurred. The AL reached a minimum value of -1300 nT by 2044 UT.

Auroral observations. Plate 2a shows the auroral observations corresponding to the event in question. Prior to the new onset the auroral distribution had the characteristic double oval configuration associated with substorm recovery phase with omega bands in the east near Tixie (5 MLT). >From 2005 to 2009 UT periodic forms on the main UV oval developed between 23 and 7 MLT (spanning 8 hours of local time). Larger-scale brightenings prior to onset occurred near 2 MLT at 2009 UT (right top panel) similar to previous observations [Shepherd and Murphree, 1988]. The poleward expansion and formation of a bulge occurs between 2009:13 and 2010:12 UT from the location of previously existing AAFs on the peak of main UV oval. Note that at 1 min time resolution there is no evidence in this case for a fading of arcs prior to onset as has been observed on other occasions [Pellinen and Heikkila, 1978]. The AAFs at 2 MLT also brighten along with the bulge indicating a similar and large scale process extending over

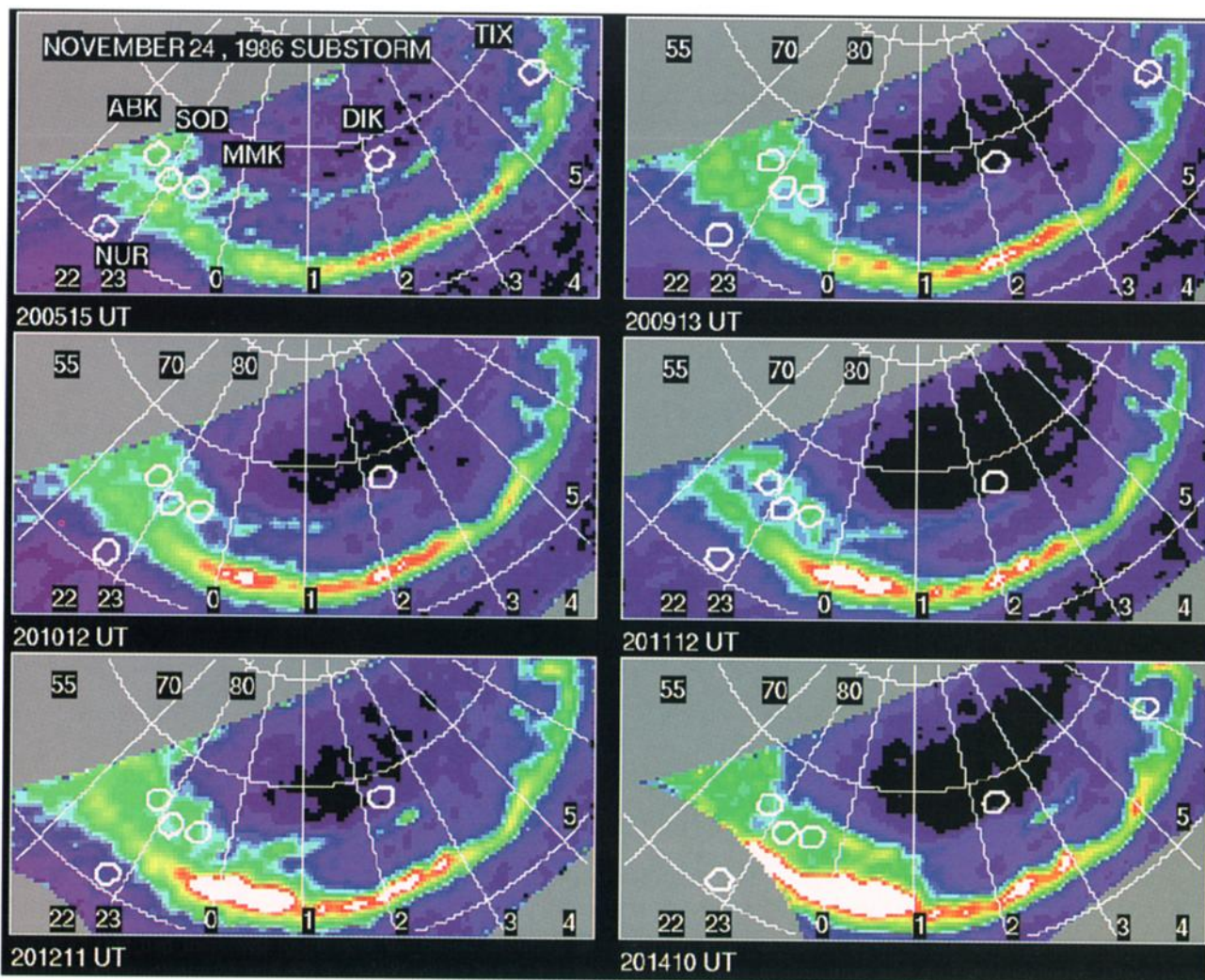


Plate 2. (a) Images showing AAFs, omega bands and substorm onset during a double oval event on November 24, 1986 between 2005:15 and 2014:10 UT. The AAFs intensify along with the onset indicating their close connection with the substorm process. Every one hour MLT is shown beginning with 22. The latitude lines are 55, 70, and 80 CGMlat. Also shown are several ground station field of views. (b) Images between 2017:29 and 2027:45 UT showing a poleward boundary (and embedded arc systems) moving southward towards the AAFs westward of the auroral surge near midnight. 22, 23, 0, and 1 MLT as well as 55 and 70 CGMlat are shown.

about 4 hours of local time. The AAFs propagate to the east (2010:12 - 2014:10 UT) while the bulge expands both east and west. At the same time omega bands can be seen to move eastward at Tixie from 2005 to 2014 UT (the speed between 2010 and 2014 UT for both of these was about 1 to 1.5 km/s). The premidnight intensifications on the other hand showed some evidence of more rapid westward movement.

At 2009 UT the mode number was about 48 near the onset location at the peak in the main UV oval. At the onset time (2010 UT) this had increased to 96 near the onset, about 72 at 2-3 MLT but was only 24 at 5 MLT. After onset (2012:11 UT) the mode number again decreased (36 near onset and 60 at 2 or 3 MLT). It further decreased to 30 by 2014:10 UT at 2-3 MLT. At the same time as this occurred some wave-like structures with a mode number of about 20 were seen at the poleward auroral boundary.

Plate 2b illustrates the further development of this substorm. AAFs can be seen westward of the surge (near 22-23 MLT the

mode number is about 60 at 2017 UT). Locally (at 21-23 MLT) the poleward boundary of the aurora begins to retreat equatorward. At 0-1 MLT on the other hand a rapid poleward motion occurs between 2019 and 2024 UT with a surge developing at the west end of this motion. The spiral forms to the west of surge drift eastward during this interval. These spirals wind up counterclockwise when viewed in the direction of the magnetic field (LH sense) as one might expect from an upward field-aligned current perturbation [Hallinan, 1976]. Multiple arcs aligned with the oval west of the surge and poleward of the AAFs appear at this time and drift equatorward. These may be triggered by processes in the plasma sheet boundary layer (PSBL) activating and propagating earthward. This is opposite to the direction observed by Nielsen *et al.* [1993] but is consistent with an earthward moving source activating periodically varying field-aligned current systems [Elphinstone and Hearn, 1993].

Magnetometer observations. Lovozero showed the onset of

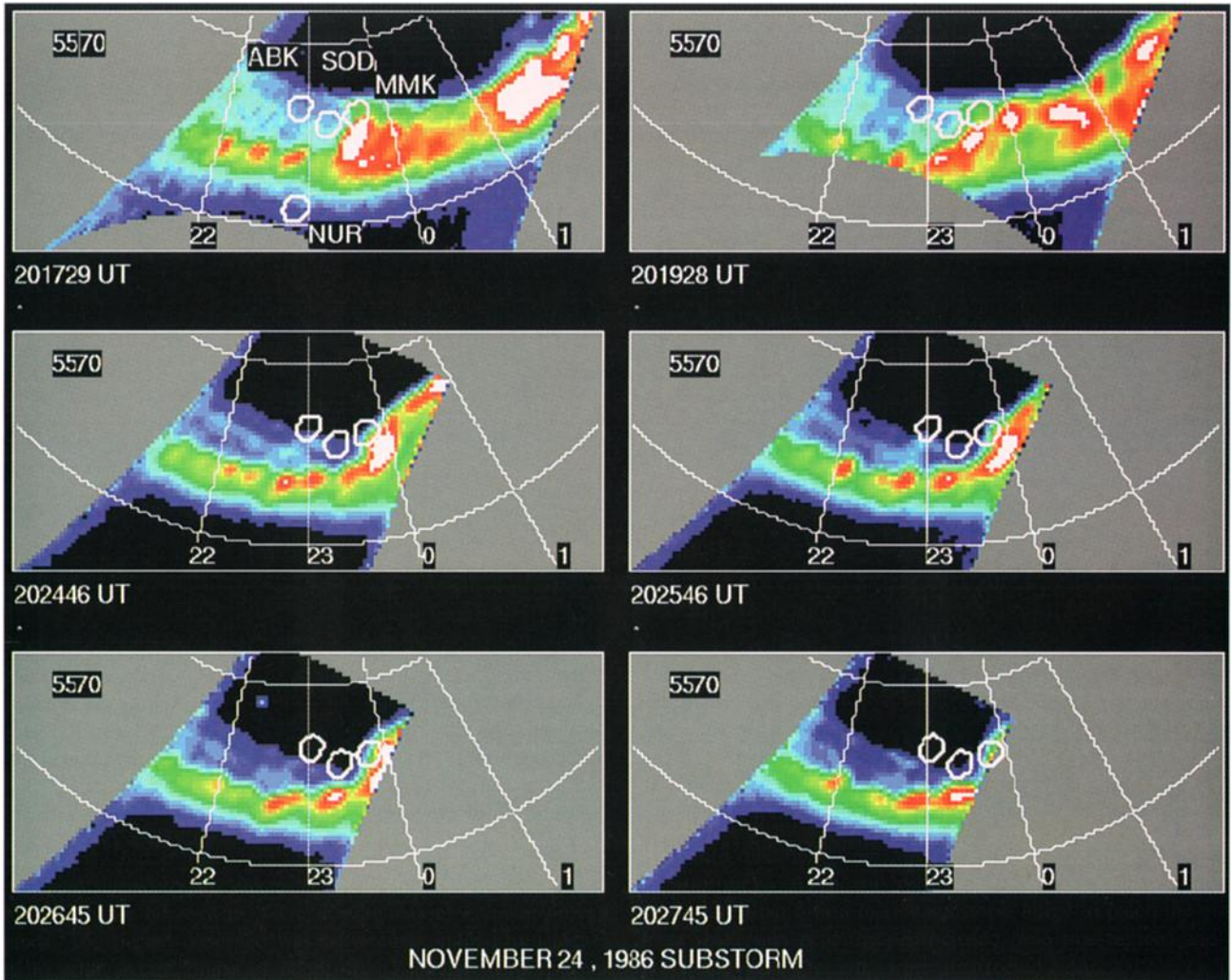


Plate 2. (continued)

weak P_i $2/P_i$ $1B$ pulsations between 2011 and 2012 UT in agreement with the explosive onset of the aurora. Note that the precursor activity did not give a clear signature. Increases in this pulsation amplitude were seen at 2013–2014 UT, 2015–2016 UT, 2017 UT, 2022 UT, and 2033 UT. Figure 3 shows the magnetometer X and Y traces from four stations. Tixie (TIK) was located near the omega bands at 5 MLT. Borok (BOX) and Nurmijarvi (NUR) were equatorward of the oval with Borok near the onset location (23.5 MLT) and Nurmijarvi to the west. Loparskaya (MMK) was located in the region of minimum intensity between the two ovals. Loparskaya, Tixie, Nurmijarvi, and Borok were all situated at local times associated with the westward electrojet before the onset. Ps 6 period pulsations can be seen at Tixie in association with the omega bands. The period observed was between 6 and 10 min (1.5–3 mHz) with an amplitude of about 40 nT in the X component and to a lesser extent in the Y component. Tixie was beneath and equatorward of the westward electrojet but poleward of main UV oval (X and Z components negative). The pulsations in the X component leads the Y so they have a clockwise sense (i.e., right-handed (RH) polarization). This is consistent with an eastward propagation (the same motion as that of the omega bands) if paired Hall current loops lie poleward of the station.

Borok station was located equatorward and just west of the onset location (located outside of the view included by the panel). Pulsations at 1.4 mHz (10 nT amplitude) were seen mainly in the X component prior to onset. At Nurmijarvi (west of Borok) a similar frequency was seen. Some time after onset multiple frequencies in the 1 to 10 mHz range appeared at both stations. At Nurmijarvi the Y component led X implying an anticlockwise (left-handed (LH) polarization) and westward propagation sense. This is also consistent with the motion of the AAFs near this station. This direction is further confirmed by delays between the high latitude stations which also imply a westward direction (from MMK to Kevo to Kilpisjarvi).

Summary. As noted by *Elphinstone and Hearn* [1993] it took more than 6 min for the substorm bulge to reach the outermost oval (i.e., near the open-closed field line region) and the inner and outer regions were unaffected until 2017 UT. This was a double oval onset with the onset beginning at the peak of the main UV oval during a time of enhanced ring current. Long-period pulsations were seen both near the onset location (in association with AAFs) and near the omega bands. The motion was westward at preonset local times but eastward propagation occurred postmidnight. The mode number was again observed to change to higher values close to the onset time. A

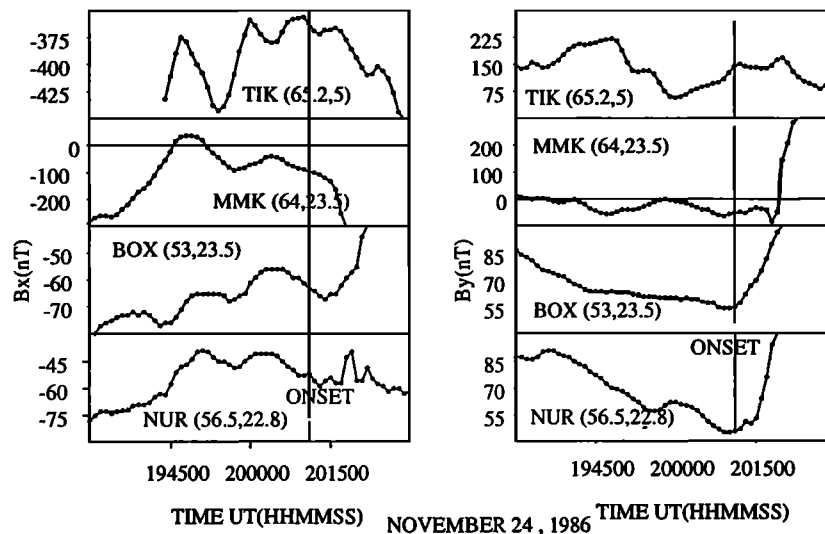


Figure 3. X and Y ground magnetic field data for TIK, MMK, BOX, and NUR for the event in Plate 2. Long-period pulsations are evident.

lower wavenumber was seen in the morning in combination with a higher frequency. The observed speed is fairly consistent with a frequency of 1.4 mHz and a mode number of 24. In the magnetosphere this would be a speed of about 2L to 3L km/s or quite similar to the first example shown in this paper. Note that in this case however the mode number and frequencies were quite different. AAFs were seen both west and east of onset. Once the disturbance reached the most poleward edge new arc systems drifted equatorward toward the AAFs.

2.3 Substorm During the Recovery Phase of a Previous Substorm: Orbit 1177 (September 23, 1986)

This event shows the recovery phase of one substorm (characterized by the double oval configuration) superimposed on dayside growth phase activity which shifts to the nightside, eventually being associated with an AAF onset.

Geophysical conditions. This event occurred during a storm which began in association with a large solar wind pressure change on the previous day. The Dst was less than -40 nT for 12 hours previous to the beginning of the event at about 2030 UT. The AU index reached more than 200 nT, while the AL index was in recovery from a -800 nT substorm which began at about 1830 UT. It recovered to about -100 nT at which time the event in question resulted in a new 750 nT decrease.

IMP 8 was located at $x_{GSE} = 33 R_E$, $y_{GSE} = -11.9 R_E$, and $z_{GSE} = -13.6 R_E$. IMF B_z turned negative briefly at 2027 UT and then for an extended time after 2029 UT. With an average speed of 660 km/s one might expect the first B_z change at the subsolar point at about 2031 UT and the second by 2033 UT. The preonset sector aurora turned on briefly at 2031:18 UT and then again at 2038 UT at which time fan arcs developed in an antisunward and poleward direction reaching ≈ 4 MLT by 2043 UT [Elphinstone *et al.*, 1991a]. The first brightening near the nightside onset took place just prior to 2047:29 UT. IMF B_y was negative and B_x positive consistent with the observed morning sector polar arcs. There were numerous solar wind pressure changes throughout this time which had an average solar wind density of 4.6 cm^{-3} . These changes were typically about 15% except for two notable exceptions at 2034-2035 UT and at 2046-2047 UT where the pressure changed by 90% and

104%, respectively. The first could have played an active role in the development of the fan arcs and the brightening of the nightside arcs systems. This would imply a time delay from the satellite to the low-latitude nightside of 12.5 min. It seems unlikely therefore that the second pressure pulse had any influence on the night sector until about 2059 UT.

Auroral and magnetic observations. Plate 1 in Elphinstone *et al.* [1991a] illustrated the dayside precursor followed by the development of the fan arcs and the substorm onset deeply embedded within the closed field line region. Plate 3 in the current paper focusses on the temporal development of the nightside sector between 2043 and 2056 UT. In the upper left panel at 2043:51 UT a "quiet" double oval can be seen with one set of arcs at about 70 CGMlat and the main UV oval at about 63 Mlat. In the next panel at 2047:49 UT a region spanning about 2 hours local time in the morning sector has brightened to form a set of AAF intensifications (m is about 72). The bright region to the far west at 1 MLT is the region which eventually forms into a WTS. Over the next 5 min the wavelength of the disturbance changes from $m = 72$ (2047:49 UT) to $m = 96$ (2049:47 UT) and back again to $m = 48$ (2050:47 UT).

An interesting change takes place at 2051:46 UT near 1.5 MLT. At this time there is a division between the newly forming intensification and the region to the east. Between 2051:46 and 2053:45 UT the disconnection becomes very clear and results in the arc system furthest to the east (2 MLT) lying equatorward of the substorm bulge region (1 MLT). This apparent separation moves about 0.5 MLT over 119 s indicating an eastward velocity of 3.2 km/s on the ground (at 63 Mlat). At the same time as this occurs the auroral "horn" forms to the west of the 1 MLT activation and by 2053:45 UT a well-developed WTS has appeared deeply embedded in the closed field line region. The westward motion began coincident with Lovozero and Borok ground magnetometers registering Pi 2 activity (see below). It may be that the eastward motion of the split coincides with the downward current of the substorm current wedge (SCW) and the surge with the upward portion. If this is the case then we can identify the very first indication of the SCW to be an ionospheric region which is about 380-500

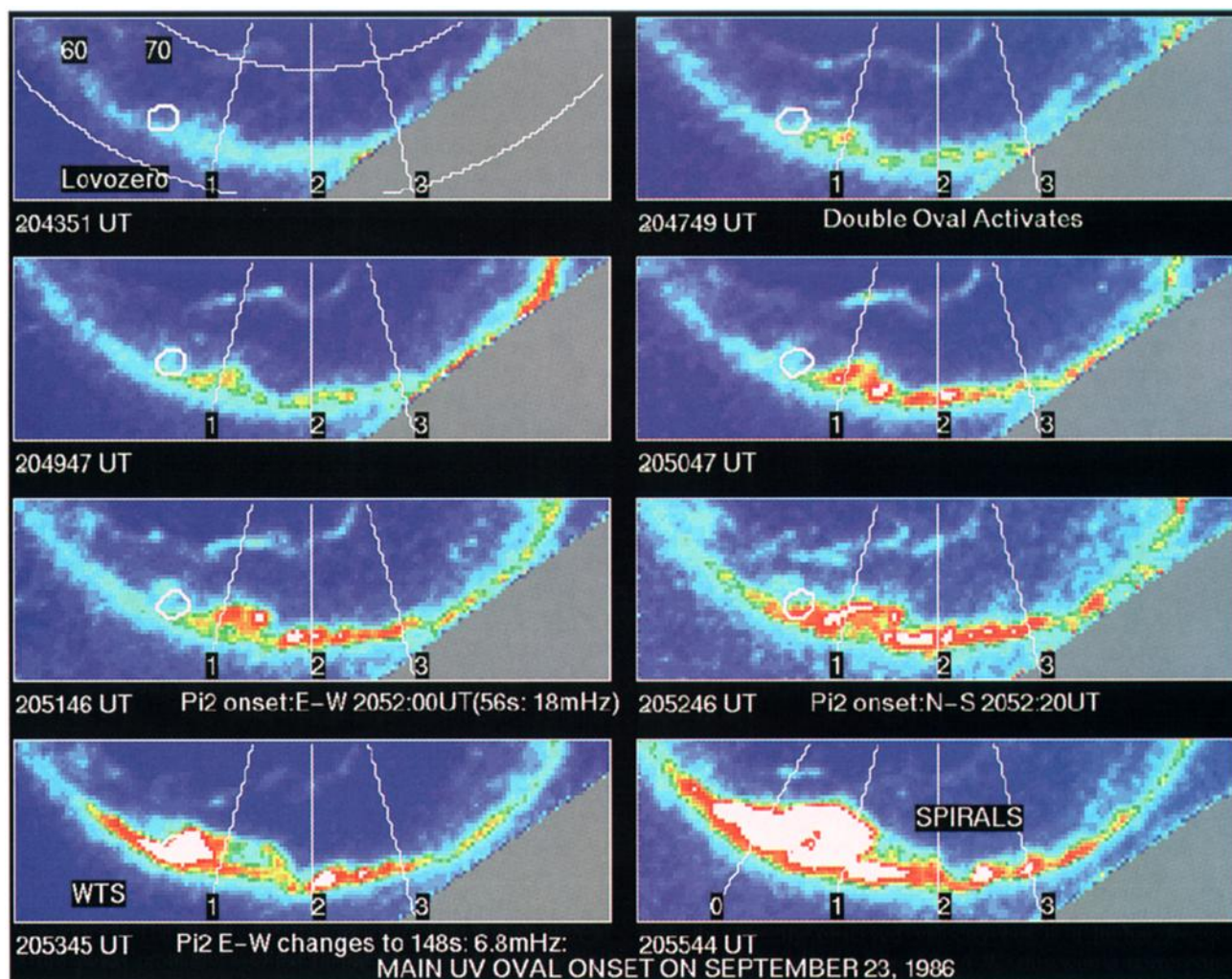


Plate 3. Images on September 23, 1986, between 2043:51 and 2055:44 UT which show AAFs developing prior to strong Pi 2 activity and substorm expansion. The last panel shows AAFs can be periodically spaced auroral spirals.

km across (i.e., not a pointlike event). This is consistent with the initial substorm wedge size reported by *Baumjohann et al.* [1981].

At the time of the main Pi 2 onset (2051-2052 UT) the AAF intensifications cover a local time range from 23.5 MLT to about 6 MLT. At 2052:46 UT (between 2 and 3 MLT) the mode number is about 100 while slightly later it is has reduced to about 50 (2055:44 UT). All-sky camera data at Loparskaya registered activations at about 2019, 2036, and 2050 UT (coinciding with some pulsations in the Pi 2 range) with breakup occurring at 2052-2053 UT (A. Yahnin, private communication, 1994).

Summary. The southward turning of B_z combined with a pressure pulse probably resulted in the fan arcs prior to onset. This auroral pattern spread from about 9 MLT to the region of onset over about a 10-min period. It may be linked to wave activity within the magnetospheric cavity associated with the solar wind pressure pulse. At this time, AAFs appeared close to midnight. These occurred prior to the main Pi 2 activity on the ground. The onset again began from the peak in the main UV oval during a double oval event (i.e., recovery phase of a previous substorm), and the resulting bulge took about 5 to 10 min

to reach the outermost system of arcs (probably associated with the PSBL). This shows that it is incorrect to attribute the substorm bulge to a distortion of the separatrix between open and closed field lines as has previously been proposed [Lyons, 1991].

As in the previous event, the mode number (the number of wavelengths in 2π rad) increased towards onset time ($m = 100$) and decreased after ($m = 50$). The Pi 2 pulsation seen at Lovozero is LH elliptically polarized in the azimuthal direction and changes frequency from 18 mHz (when $m = 84$) to 6.8 mHz (when $m = 48$). The implied velocity changes from $8.6L$ to $5.7L$ km/s (3.9 to 2.6 km/s at 63 Mlat). This is consistent with the directly observed velocity but is a higher frequency than the previous examples. At $6 R_E$ this would correspond to a speed of 30-50 km/s. This should be the approximate speed at which the disturbance and the current wedge is growing azimuthally.

In this case a well-defined WTS formed on the main UV oval deeply embedded within the closed field line region. Spiral forms were associated with each of the azimuthally spaced intensifications. The sense of these spirals is opposite to that of the flow vorticity in a Kelvin-Helmholtz instability

associated with an upward field-aligned current. It is in the correct sense to what one would expect from the magnetic vorticity associated with the upward current [Hallinan, 1976].

2.4 Quiet Time Substorm After Large Growth Phase and Magnetospheric Compression: Orbit 0842 (July 24, 1986)

A coronal streamer passed the Earth some hours prior to the event but did not trigger the substorm/storm. Instead, IMF B_z turns southward and strong growth phase activity is seen in the aurora prior to an AAF onset. CCE is located in the local time sector of onset and can be used to compare various optical observations with their high altitude signatures.

Geophysical conditions. For this event the IMP 8 satellite was located at $x_{GSE} = 19 R_E$, $y_{GSE} = 27 R_E$, and $z_{GSE} = -11 R_E$. Between 1640 and 2106 UT there were five major solar wind pressure increases which altered the pressure by a factor of 5.4 by 1944 UT compared to what it was at 1500 UT. Image data taken after the first impulse indicated a relatively quiet auroral distribution. During this interval, IMF B_z was generally northward although there were three intervals of about 1 hour each when B_z became southward. At the time of these changes the total magnetic field was anticorrelated with the pressure but gradually increased towards 2300 UT. A. T. Y. Lui et al. (An auroral substorm on July 24, 1986, submitted to *Journal of Geophysical Research*, 1995) (hereinafter Lui et al., submitted manuscript, 1995) interpreted this first pressure change as being due to a coronal streamer. For this first interval the IMF was in an away garden hose configuration while after the pressure changes had occurred it was in a towards sector orientation.

Closer to the time period of interest here (≈ 2200 – 2300 UT) the average solar wind speed was 380 km/s, and the total B field was about 15 to 20 nT. IMF B_z turned negative at 2157 UT and became increasingly negative until about 2240 UT when it was less than -20 nT. After the time when IMF B_z became southward there was a solar wind pressure decrease and then increase between 2221 and 2225 UT. This corresponded to about a 50% change in solar wind pressure. When this occurred the total magnetic field was correlated with the pressure rather than anticorrelated (as was the case in the more major changes previously). This was followed by three other pulses with changes of $\approx 20\%$ at 2232, 2245, and 2252 UT. The primary difference between the time period 2200–2300 UT and the previous times was that the IMF polar angle was directed strongly southward.

The Dst had been close to zero for about 2 days previous to this event. It began a positive excursion at about 1600 UT reaching +40 nT by 2000 UT at which time it began to decrease, going negative by 2300 UT. This seems to be closely related to a compression of the magnetosphere at this time which would enhance the magnetopause currents and cause a positive excursion in the Dst .

The AU index which had been less than about 50 nT for the previous 24 hours then began to increase at about 1600 UT. It reached a plateau (≈ 100 nT) by about 1830 UT. After 2000 UT it began a gradual decrease to about 50 nT by 2200 UT. This seems to fit relatively well with the observed changes to the solar wind pressure over the previous 7 hours when the IMF was in a garden hose away configuration. After this time, AU began a slow increase and then increased abruptly at 2220 UT to over 300 nT. The index then decreased to about 170 nT by 2244 UT before a new increase at about the time of substorm onset.

The AL index was quiet (> -100 nT) for 9 hours prior to a

minimum (< -200 nT) which occurred beginning at about 2221 UT and reached its minimum value by 2236 UT. Another abrupt change occurred at 2300 UT which resulted in an AL index of < -700 nT by 2330 UT. It appears that even though there were very large pressure changes taking place before 2200 UT these did not trigger a large substorm and only resulted in changes to the eastward electrojet system. The first change to the AL index at 2220 UT seems relatively consistent with the IMF B_z turning southward and appears to be a precursor to the subsequent auroral activations.

Auroral and magnetic observations. Viking auroral data for this event are shown in Plate 4. As mentioned elsewhere [Elphinstone et al., 1991a; Lui et al., submitted manuscript, 1995] this onset was preceded by auroral activations in the prenoon sector beginning at 2236 UT. This is consistent with the 50% change in solar wind pressure which occurred at about 2221 UT. In the first panel of Plate 4 the first signs of the AAFs can be seen between 2 and 4 MLT. Over the next 2 to 3 min the form at 3 MLT can be seen moving eastward and the mode number is about 48 (i.e., at 2252:35 UT five regions of enhanced luminosity exist between 2 and 4 MLT corresponding to four waves and a mode number of about 48). The forms became more active by 2255 UT and had spread to almost 0 MLT by 2257 UT. The whole dawn auroral oval appears to have intensified by this time. The mode number increased to about 60.

At 2259:39 UT an auroral brightening appeared in the westernmost portion of the image and the aurora between 0 and 1.5 MLT has faded (this example is consistent with the Pellinen and Heikkila [1978] observations). The auroral activation moved towards the east and between 2300:39 and 2301:40 UT intensified. Also at this time, the AAFs between 2 and 5 MLT have intensified. The main brightening spanned about 1 hour local time and faded by 2303:41 UT. A new intensification occurred by 2304:41 UT and resulted in a definite poleward motion of the aurora. After this the mode number decreased to about 24 (see the last two panels of Plate 4).

If one uses the first auroral arc brightening as substorm onset then this would probably have occurred some time between 2254 and 2257 UT. If a major brightening is the defining characteristic then the time would be 2301:40 UT. If instead one uses the start of the poleward motion then the time would be between 2304 and 2306 UT. The time of onset could vary in this example over 12 min depending on which onset definition is used. Lovozero registered the beginning of weak Pi 1 pulsations at 2250 UT which increased in amplitude at 2254–2255 UT, again at 2302 UT and again at 2304–2305 UT. Note that the associated pattern is quite different in each case.

The large circles in Plate 4 represent ground station field of views at Sodankyla, Murmansk, and Dixon (45 zenith angle field of views at 120 km altitude). The magnetometer data from these stations are shown in Figure 4. The left panels show the X component change beginning at about 2222 UT. This is mostly strongly seen at the more eastward stations with the other stations not responding as strongly. The pulsations at Dixon in the X component had a frequency of about 2.2 mHz before and 3.2 mHz after 2301 UT. The Y component showed a slightly higher frequency of about 2.8 mHz.

CCE observations. Also shown in Plate 4 are the Tsyganenko [1987, 1989] field model projections of the CCE high-altitude spacecraft (apogee at about $8.8 R_E$). These show that the spacecraft was located in the vicinity of the AAFs near 2 MLT. The fact that the mappings put the spacecraft pole-

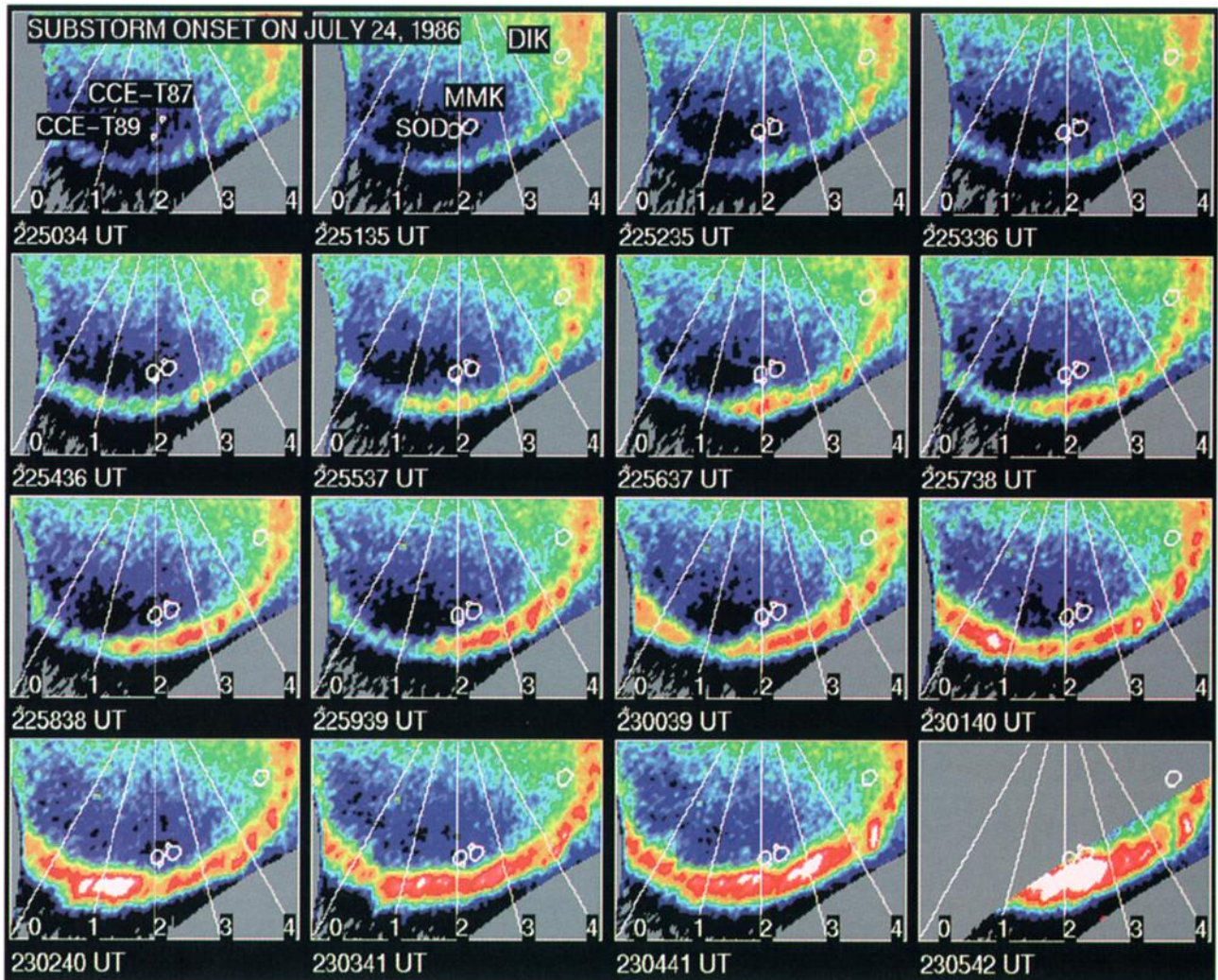


Plate 4. Images on July 24, 1986, between 2250:34 and 2305:42 UT illustrating the growth phase evolution of AAFs. The upper left panel shows the projection of CCE into the ionosphere using T87, T89 models. The second panel shows the locations of the three ground stations shown in Figure 4.

ward of the auroral zone is an indication of just how stretched the field configuration is at that time. This is supported by CCE magnetic field observations. In order to get the projected location of CCE close to the oval it was necessary to move the inner edge (x_w) of the current sheet inward by $2 R_E$, increase the tail current by 2, increase the ring current by a factor of 1.25 and thin the current sheet down to $0.5 R_E$. This indicates that for this event the tail became extremely stretched just prior to onset and that static statistical magnetic field models were not applicable at this time.

The CCE ion data for this event have been studied in some detail by Lui et al. (submitted manuscript, 1995) and the electron data are shown in Figure 5. If one uses the ion injection as a definition of substorm onset then this occurs at 2301 UT corresponding to the brightening of the AAFs and just after the larger intensification near midnight. The electron data show that, approximately corresponding to the appearance of the AAFs, there was a softening of the electron spectrum while the overall density remained unchanged. The flux change for electrons of energies > 1 keV occurred in two steps. The first change was an order of magnitude decrease in 150 ms at

2254:34 UT, while the second occurred over the next 20 s. In the auroral data this coincided with the general brightening of the AAFs near 2 to 3 MLT (images at 2254:36 UT and 2255:37). During this interval the 0.35 keV electron fluxes showed pulsations near 35 mHz (29 s).

The soft spectrum continued until 2301 UT at which time the spectrum hardened slowly over a 20-s time period, again with no density change. After this time the field began to dipolarize, the spectrum continued to harden until a dramatic change occurred between 2304:15 and 2305:15 UT. At 2304:15 to 2304:30 UT the electron density dropped by an order of magnitude and the shape of the electron energy spectrum was very flat between 0.1 and 4 keV. During this interval the number density increased once abruptly at 2304:55 UT but then decreased again. The fluxes recovered completely at 2305:15 UT. This time period coincided well with the third definition of substorm onset which initiated the poleward motion and the beginning of substorm expansion. At 2304:15 UT there was a strong change in the pitch angle distribution of the 4 keV electrons. The fluxes which were at pitch angles away from 90 deg dropped by a factor of 4 over 6 s leaving a pancake-shaped

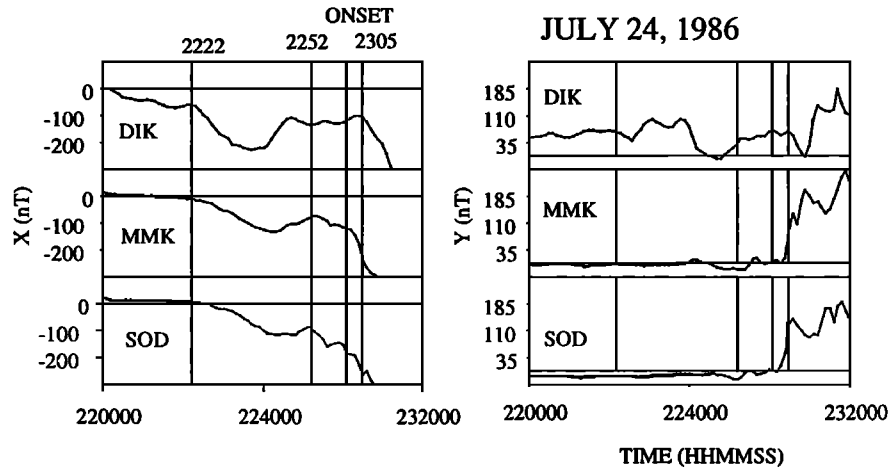


Figure 4. X and Y ground magnetic field data for DIK, MMK, and SOD for the event in Plate 4. Long-period pulsations are evident.

distribution limited to that particular energy. This was the initiation of the flux dropout associated with the substorm expansion on the ground. The field further dipolarized at this time. Events of this type have previously been noted [Lui *et al.*, 1992] in association with current disruptions in the tail.

Summary. Very large pressure changes in the solar wind were insufficient to trigger a major substorm when the IMF polar angle was northward. It was only after the combination of a pressure change with the IMF directed dominantly southward was the storm/substorm triggered. The *AL* index was driven by the IMF *B_z* southward turning while the *AU* appeared

to be controlled by both the pressure and the IMF polar angle. The first auroral activity was seen on the dayside at a time consistent with the pressure change and then propagated toward the nightside [Elphinstone *et al.*, 1991a]. The AAF activations appeared after this on the nightside and were related to both the enhanced westward electrojet (presumably due to the IMF *B_z* being southward) and to solar wind pressure changes. It was only after IMF *B_z* turned southward and another pressure pulse occurred that a major substorm was triggered. The unloading aspect of the event did not begin until 1 hour after *B_z* had turned southward and occurred in conjunction with a precursor

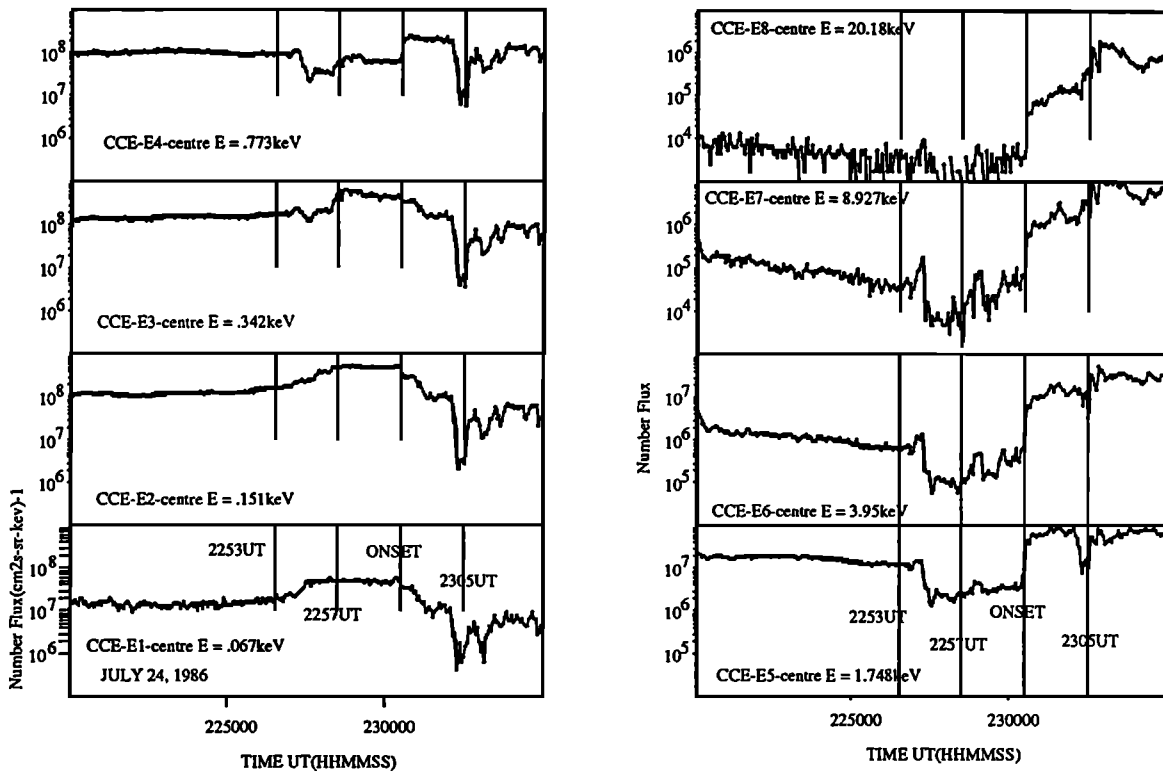


Figure 5. CCE electron number flux versus universal time in the vicinity of the azimuthally spaced auroral forms (AAFs). The center energy of each channel is shown for each plot. The vertical line show times of interest based on the auroral data of Plate 5.

growth of azimuthal wavelike structures in the early morning sector aurora. These may have been triggered by a compressional wave propagating within the magnetospheric cavity after the last pressure pulse. The AAFs had a time-dependent mode number and they propagated toward the east (sunward). They were accompanied by ground magnetic pulsations in the Pc 5 range which also propagated eastward and began at about the same time as the AAFs.

This example shows the ambiguity in onset time based on different definitions whether at high altitude or on the ground. Optically, three separate definitions could have been used. The first would be the time of the first arc brightening. This would lead to problems in defining what local time to confine oneself to. The second definition would be the time of large brightening near midnight which began prior to 2300 UT. This began slightly earlier than the dispersionless injection seen at CCE. The latter signature was probably associated with the AAFs activating near 2 to 3 MLT. The third definition corresponds to the major poleward motion which is followed by a well-defined optical expansive phase, by westward electrojets activating and by electron distribution function and density changes at CCE altitudes.

Observations at CCE showed that the three different periods optically coincided with three distinct electron signatures at high altitude:

1. A very abrupt softening of the electron spectrum was observed with no electron density change.
2. A nearly dispersionless ion injection was observed after the brightening was seen to the west and a gradual hardening of the electron spectrum occurred over a 20-s period. Again no electron density change was seen.
3. An order of magnitude change to the electron density occurred which was accompanied by a flat shape to the electron energy spectrum between 0.1 and 4 keV. This was preceded by a change to a trapped pancake-shaped distribution in the 4 keV electrons.

2.5 Substorm After 40 Min of Onset Precursors: Orbit 0855 (July 27, 1986)

Multiple eastward-moving arc brightenings during a double oval distribution culminate with an AAF onset. These optical observations are compared with onset signatures at geosynchronous altitudes.

Geophysical conditions. The *Dst* was at about -20 nT prior to this event but dropped briefly (for about 2 hours) to -40 nT after the main auroral onset near 0830 UT. Both the *AL* and *AU* were active throughout the time period between the July 24 event (see above), and this one which occurred at about 0800 UT on July 27, 1986. Between 0700 and 0800 UT the *AU* index was less than 100 nT, but shortly after 0800 UT it increased reaching more than 400 nT by about 0930 UT. The *AL* index remained greater than -200 nT up until 0830 UT at which time it began a decrease which peaked at about -1600 nT by about 0930 UT. There was no IMF available for this event.

Auroral observations. The dayside auroral distribution became active first near 14 MLT at about 0647 UT. The activity began somewhat later in the morning sector and an auroral activation occurred on the main UV oval at about 0715 to 0716 UT. This activity was not evident in the *AL*, *AU*, or *Dst* indices. Between 0730 and 0737 UT auroral brightenings occurred in the 21 to 0 MLT sector. By 0730 UT a double oval distribution had developed along with 14 MLT spirals, candi-

date flux transfer events (FTEs) and morning sector fan arcs [Elphinstone *et al.*, 1993b]. The dayside auroral distribution indicated an IMF B_y negative configuration with the morning sector oval near noon being displaced poleward of the dusk sector aurora. Plate 5 shows the nightside auroral distribution between 0745 and 0830 UT. In this event there were four separate auroral activations which occurred in the night sector prior to a well-defined substorm onset beginning at 0829 UT. These occurred at 0730, 0747, 0811, and 0820 UT with finally a major optical onset occurring at 0829 UT.

The second intensification began at 0744 UT with a bifurcation and brightening of an arc system near 20 MLT. This consisted of a rapidly moving eastward intensification on the most equatorward or main UV oval (top left panels of Plate 5). By 0751 UT this intensification had begun to fade. At 0800 UT the main auroral arc systems formed a continuous band (with intensity variations) between 21 and 0 MLT and seemed to be coincident with the poleward edge of the auroral distribution. By 0808 UT, however, the auroral distribution had again split into two distinct regions. A new activation began at 0811 UT from the west and originated from the poleward edge of the most equatorward set of arcs. Over the next 10 min the activation did not reach the most poleward system as a substorm bulge but by 0818:57 UT arc systems connected the two ovals (near 21 MLT).

Then at 0820 UT a new arc system brightened again from the west towards the east (last panel of third row in Plate 5). This system then developed into a westward traveling spiral form which lay deeply embedded within the closed field line region. (This spiral form can be seen in the lower left panels of Plate 5 as a localized bright spot near 21 MLT on the most equatorward oval. Using different resolution this activation can clearly be seen to be a spiral form.) From an all-sky camera view this form would probably be labeled a WTS. This spiral moved westward and arc systems moved up to the most poleward arcs of the double oval. At the same time at 0828 UT a new auroral system brightened to the east. This developed into a major optical substorm beginning at 0829 UT (defined by a substorm bulge which envelopes the entire latitudinal extent of the auroral distribution at midnight). AAFs were observed in the onset region between 0828 and 0830 UT (see also Plate 9).

High- and low-altitude satellite observations. In addition to the auroral data both low- and high-altitude satellite observations were available. In Plate 5, specific points along the DMSP-F7 trajectories for two orbits are shown by small circles near 22 MLT. These points correspond to the CGM coordinates of the satellite footprint at 120 km altitude in the northern hemisphere and correspond to boundaries determined using the neural network of Newell *et al.* [1991]. The field model used was Tsyganenko [1987] (T87) with $K_p = 3$. The path at earlier local times corresponds to the oval crossing between 0736 and 0745 UT while the other one corresponds to a southern hemisphere crossing between 0815 and 0820 UT.

Three points are labeled in the earlier crossing. The most poleward point (labeled 1 in Plate 5) corresponds to the most poleward extent of the upward field-aligned current and the low-altitude boundary plasma sheet (LABPS). This corresponds relatively well to the poleward edge of the double oval. Point 2 in Plate 5 shows the location of the poleward edge of the low-altitude central plasma sheet (LACPS) as well as the poleward edge of the region 2 field-aligned current. In this example the poleward portion of the LACPS alternates with two additional LABPS signatures. This is consistent with the

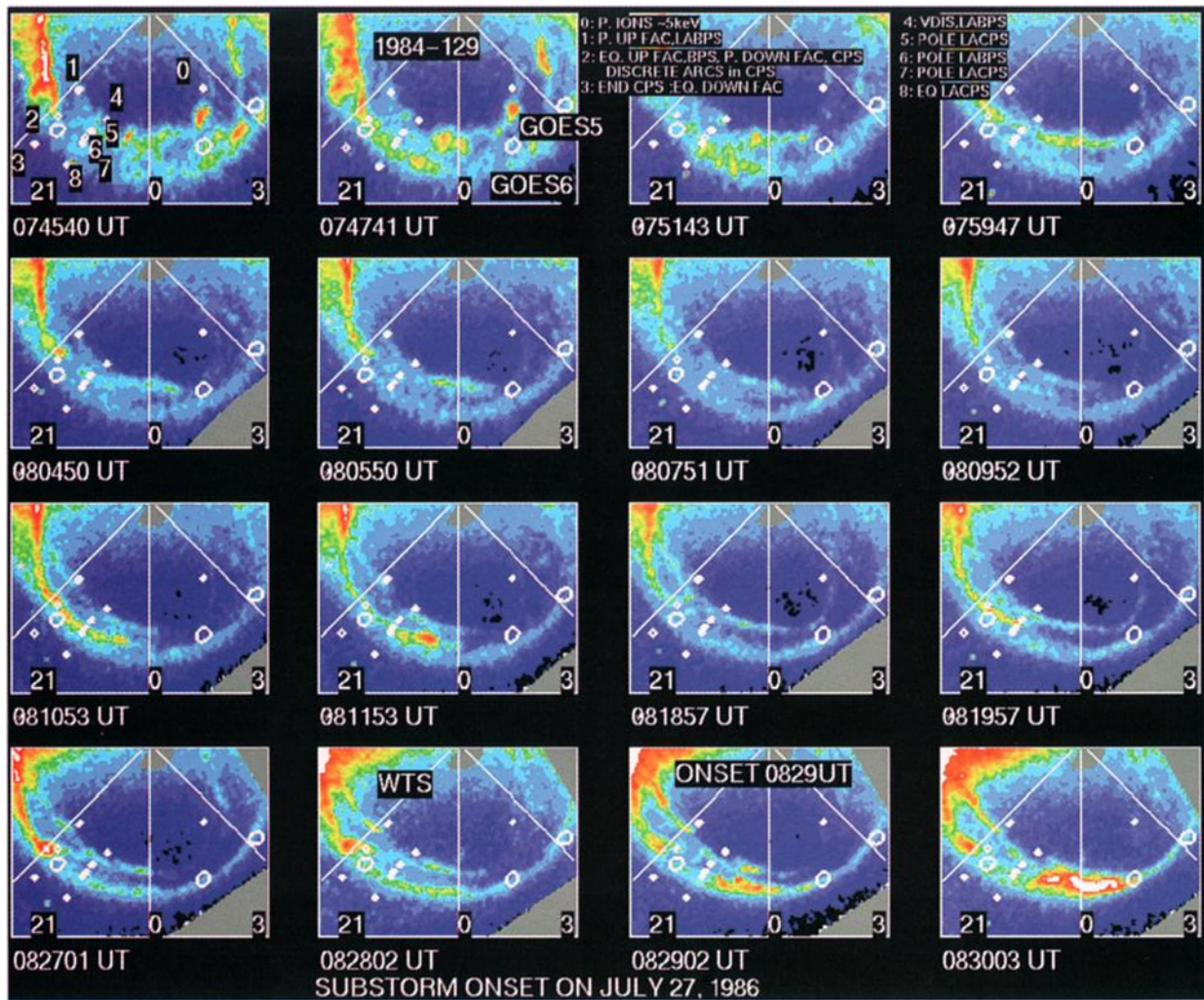


Plate 5. Images on July 27, 1986, between 0745:40 and 0830:03 UT illustrating the multiple intensifications which lead up to an AAF substorm onset. 21, 0 and 3 MLT are shown. The small white circles (points 1 to 8) represent particle boundaries seen by DMSP-F7 (projected to the northern hemisphere at 120 km altitude in CGM coordinates). Points 1 to 3 correspond to observations between 0739 and 0745 UT. Points 4 to 8 were acquired from 0815 to 0818 UT. The corresponding legend is shown at the top of the Plate. The large circles show from left to right the T87 projections of the 1984-129, GOES 6 and GOES 5 satellites.

arc systems observed in the main UV oval at this time and shows there are two distinct source regions for discrete auroral arcs. Point 3 shows the location of the equatorward edge of the LACPS and the region 2 field-aligned current. This matches reasonably well with the equatorward edge of the main UV oval.

The two source regions for the discrete arcs are further substantiated for the southern hemisphere crossing near 0815 UT (Plate 6). For this crossing there are two distinct auroral arc regions one near the poleward boundary (0817:20 to 0818:17 UT and points 4 and 5 in Plate 5) and another embedded within the LACPS precipitation between 0816:29 and 0816:50 UT (points 6 and 7). These observations correspond approximately to the auroral data shown in the last two panels of the third row in Plate 5. These low-latitude arcs occur at the poleward edge of the region where the ions have an energy dispersion to lower energy as one moves equatorward. This location probably corresponds to the inner edge of the high-altitude central

plasma sheet. The most poleward arcs occur just equatorward of a velocity dispersed ion signature (VDIS) which may represent the mapping of the high-altitude plasma sheet boundary layer (PSBL). For this example the average energy and energy flux of the electrons showed two peaks corresponding to the two active regions of the double oval. The ions showed a monotonic increase in energy and energy flux up to the inner edge of the central plasma sheet (point 7 in the Plate 5) at which time they both began to decrease.

The Viking spacecraft passed over the auroral zone closer to 3 MLT (point 0 in Plate 5). This point shows the location at which Viking recorded the poleward boundary of about 5-keV ions indicating this is a reasonable location for the closed field line boundary in the morning sector. This corresponds to the poleward edge of the faint double oval structure also seen there.

The above observations support the contention that the substorm onset is originating within the region 2 field-aligned current system, near the Earth, probably close to the inner por-

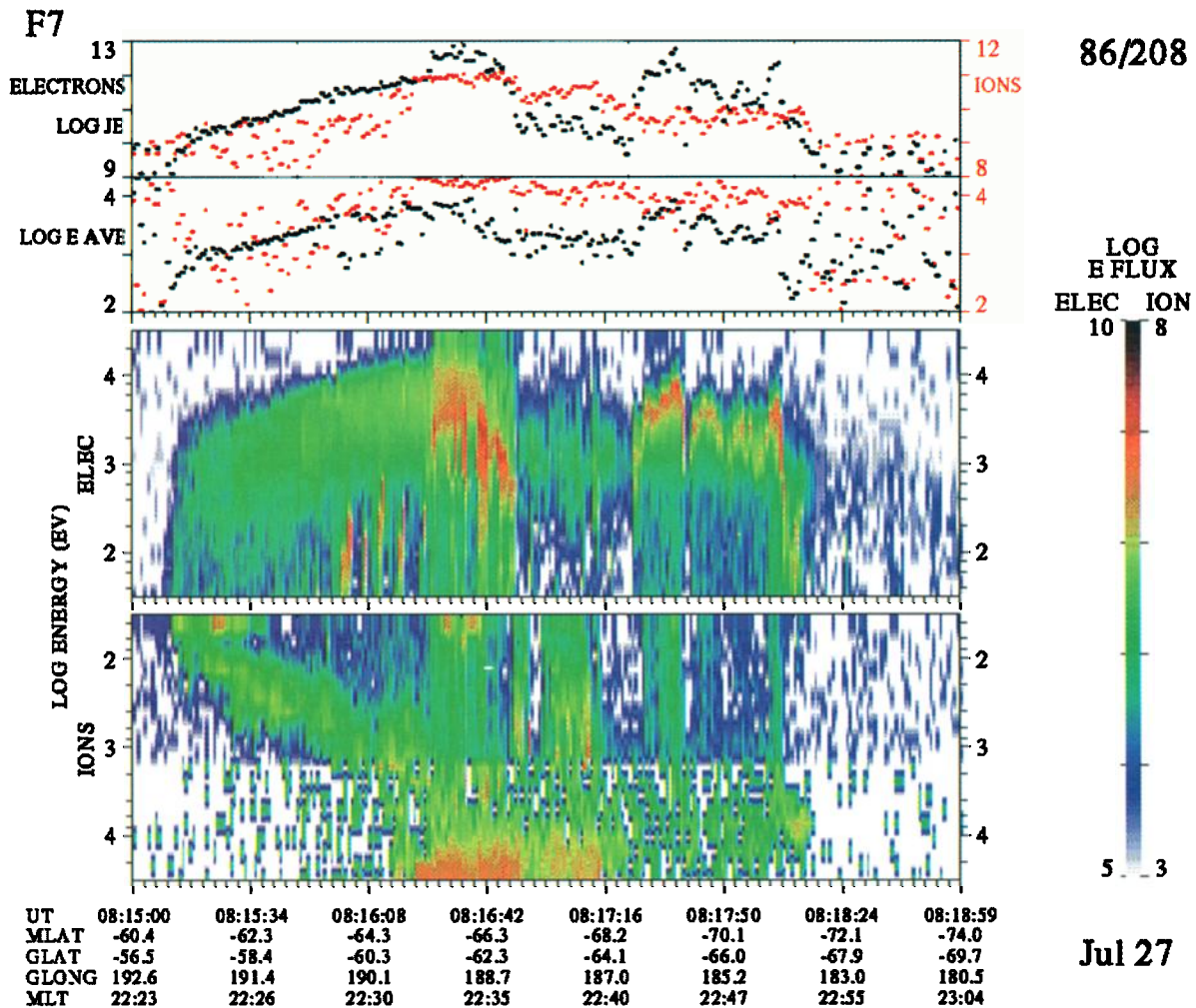


Plate 6. DMSF-F7 spectrogram showing two sources of discrete auroral arcs. The most poleward system lies at the inner edge of the VDIS while the other one lies at the poleward edge of where the ion energy begins to decrease with decreasing latitude. The latter is associated with substorm onset.

tion of the tail current sheet. Since the inner edge of the central plasma sheet is not a sharp boundary this location corresponds to the tailward portion of this inner edge. In addition to the low-altitude observations there are also observations from three geosynchronous orbit satellites. These have been projected to the ionosphere using the T87 field model ($Kp = 3$) and are shown as large circles in Plate 5.

The Los Alamos satellite 1984-129 was located in an optimal local time to record changes associated with these activations. On the basis of this and the satellite 1982-019 several injection events have been identified before and during the imaging interval. At satellite 1982-019, electron injection events were seen at 0643 and 0716 UT. The latter event was also seen as a moderate proton injection event in the 21 MLT sector (1984-129). This event was associated with the first intensification on the main UV oval from which a double oval configuration developed by about 0730 UT. The auroral activations which appeared on the main UV oval between 0730 and 0737 UT and again at 0746 UT were also associated with small electron injection events at 1984-129. At 0752 UT a small proton injection event was seen. It was not until about 0835 UT that a major injection event in both the protons and electrons took

place at all the Los Alamos satellites. This proton event was nearly dispersionless in the 21 MLT sector (1984-129) but the electron events all showed dispersive signatures. This indicates that the first events would not be classified as substorm onsets based on the particle injection definition but rather as pseudobreakups. The onset at 0829 UT took place well eastward of 1984-129 and remained eastward as it expanded.

GOES 5 and 6 provided magnetic field observations during this event and their projected locations put GOES 6 about 1.5 MLT eastward of the substorm onset location, while GOES 5 was closer to 3 MLT. These satellites recorded Pi 2 activity in the azimuthal field component associated with the event at 0748 UT. No dipolarization was seen at this time. The response at GOES 5 was delayed relative to GOES 6 by between 9 and 27 s indicating an eastward propagation speed of about 700 to 2000 km/s which is reasonably consistent with Alfvén speeds at geosynchronous orbit. The other events were not noticeable at either satellite with the exception of the main onset at 0829 UT. For this event a dipolarization and Pi 2 activity occurred somewhat later at 0830 UT at GOES 6 and even later at GOES 5 (0845 UT). This is consistent with the activations moving into the GOES 6 local time sector between 0829 and 0835 UT (see

Plate 5). Thus using Pi 2 activity at geosynchronous orbit altitude the first and last events might be considered onsets while the other events did not register in the morning sector region.

Summary. Dayside activity was followed by a nightside auroral activation which resulted in a double oval configuration. During this configuration auroral activations were observed which began in the west near 20 MLT and progressed toward the east. These occurred in intervals of 10 or 20 min and eventually led to an AAF onset and an auroral substorm. Each activation had some but not necessarily all of the characteristics of a substorm (e.g., Pi 2 activity, WTS, poleward motion) but would not have normally been classified as an optical substorm onset. This is an example of multiple activations gradually providing conditions under which a major onset could begin.

These activations began near what is probably the tailward portion of the inner edge of the central plasma sheet (i.e., near the inner edge of the cross tail current) and demonstrate that there are two distinct sources for discrete auroral arcs during a double oval configuration. The onset appeared to begin within the region 2 field-aligned current in the dusk sector.

During the interval of periodic intensifications which led up to a major optical substorm onset, weak particle injection events took place at geosynchronous orbit but no strong injection event was observed even though a westward traveling spiral did form deeply embedded within the LACPS precipitation region. A major injection event was not observed until some ten min after the onset at 0829 UT. At local times to the east of onset dipolarization was observed to occur when the optical activity reached the local times of the GOES satellites. Some eastward propagating magnetic pulsation activity (azimuthally polarized) in the Pi 2 period range was observed to occur in association with the first auroral activation.

2.6 Multiple Substorm Onsets With an Auroral Streamer Event: Orbit 293 (April 16, 1986)

This event is perhaps the most significant case study in this paper. The data sets which overlap for this AAF onset allow considerable information about the onset location to be determined (see Table 1). The optical data show auroral dynamics which indicate an AAF onset can be influenced by more tailward processes.

Geophysical conditions. The *Dst* index decreased from near 0 to about -20 nT late on April 15 and was increasing during this event (0320 to 0430 UT on April 16). Both the *AL* and *AU* indices registered a substorm beginning at about 2300 UT on April 15, 1986. The *AL* index reached a peak at about 0000 UT (≈ -400 nT), while *AU* showed a peak between 0100 and 0200 UT (≈ 150 nT). This event therefore took place during the recovery phase of a previous substorm. The *AL* index showed a new onset (≈ -200 nT) beginning at about 0430 UT. The *AU* index did not respond until about 0500 UT.

There was no solar wind data for this event although there was IMF. The IMF was in an away garden hose configuration with IMP 8 located at $x_{GSE} = 5.89 R_E$, $y_{GSE} = 33.95 R_E$, $z_{GSE} = -14.17 R_E$. There were abrupt changes in the IMF azimuth angle between 0300 and 0410 UT. The changes involved a rotation in the *x-y* GSM plane such that B_x abruptly became less negative at about the same time as B_y increased (the azimuth angle changed from near 170 to 130 deg). This new orientation lasted about 8 to 11 min at which time the field returned to its previous orientation. This occurred 3 times beginning at about 0311, 0335, and 0354 UT. The total field remained relatively unchanged during the first two intervals

from 0310 to 0343 UT. During this time period, IMF B_z turned from weakly negative to positive. At the end of the second interval (≈ 0343 to 0350 UT) the total *B* field decreased from about 6.5 nT to about 5.2 nT (20% change).

As described below it appears that there were auroral intensifications on the main UV oval, roughly corresponding to each of these intervals. Similar to the previous event these eventually led to a major optical substorm onset. In this case each event could be associated with a high-altitude substorm onset signature.

Auroral observations. Plate 7 shows the auroral distribution from 0313 to 0426 UT on April 16, 1986. The panels in the upper left show a double oval distribution with the most poleward oval being most active. Between 0313 and 0326 UT this most poleward oval develops into a large-scale stationary surge [Cogger and Elphinstone, 1992]. The surge form can clearly be seen in the image at 0337:51 UT. Over the next 30 min this most poleward system begins to fade leaving diffuse auroral precipitation poleward of the main UV oval at 0406 UT. The main UV oval on the other hand started out as a faint distribution but by 0406 UT was the main region of auroral activity. Auroral activations on the main UV oval occurred at 0319, 0331, 0340, 0354, 0406, and 0430 UT (the last activation is not shown in the Plate). The event at 0331 UT is clearly an AAF intensification. Using a delay time of 5 to 11 min, three of the pseudobreakups can be linked to the discontinuity in the IMF changing to a lower azimuth angle (i.e., towards dusk). The other events at 0331 and 0354 UT can be linked to the reverse change.

The first event (0319 UT) had AAFs associated with it and the activations moved eastward between 0320 and 0323 UT. The second activation appears to have been linked to activity which begins on the most poleward oval and moves equatorward. At 0321:45 UT, an arc system lies just equatorward of the most poleward oval. The more poleward system fades and the newly formed "auroral streamer" remains attached to the most poleward system at 22 MLT while drifting westward and equatorward at later local times. By 0325:47 UT the most eastward end has reached the main UV oval which brightens a small amount by 0328:28 UT. By 0331:08 UT an AAF has dramatically intensified on the main UV oval (last panel of second row in Plate 7). The associated mode number was between 20 and 30.

By 0337:51 UT this brightening had disappeared and the stationary surge form on the most poleward oval was well established. Between this time and 0340:31 UT an intensification on the main UV oval occurred just eastward of the stationary surge form (also eastward of the previous intensification). This faded by 0347 UT and by 0354 UT a new intensification occurred in the region to the west (near 20 MLT) of the previous activation (last panel of third row). At this local time the main UV oval was located near the poleward boundary of the aurora. This faded by 0403:39 UT and was followed by the next activation at about 0406 UT. This region of activity then moved west.

By 0425 UT (last panel) this activation had faded and the double oval was visible to the east. By 0430 a new activation had occurred (not shown). Each of these events might be labeled pseudo-onsets in that they were activations in the evening sector which did not lead to a substorm bulge formation. The *AL* index did not show a substorm occurring until the last activation near 0430 UT.

High- and low-altitude satellite observations. This event

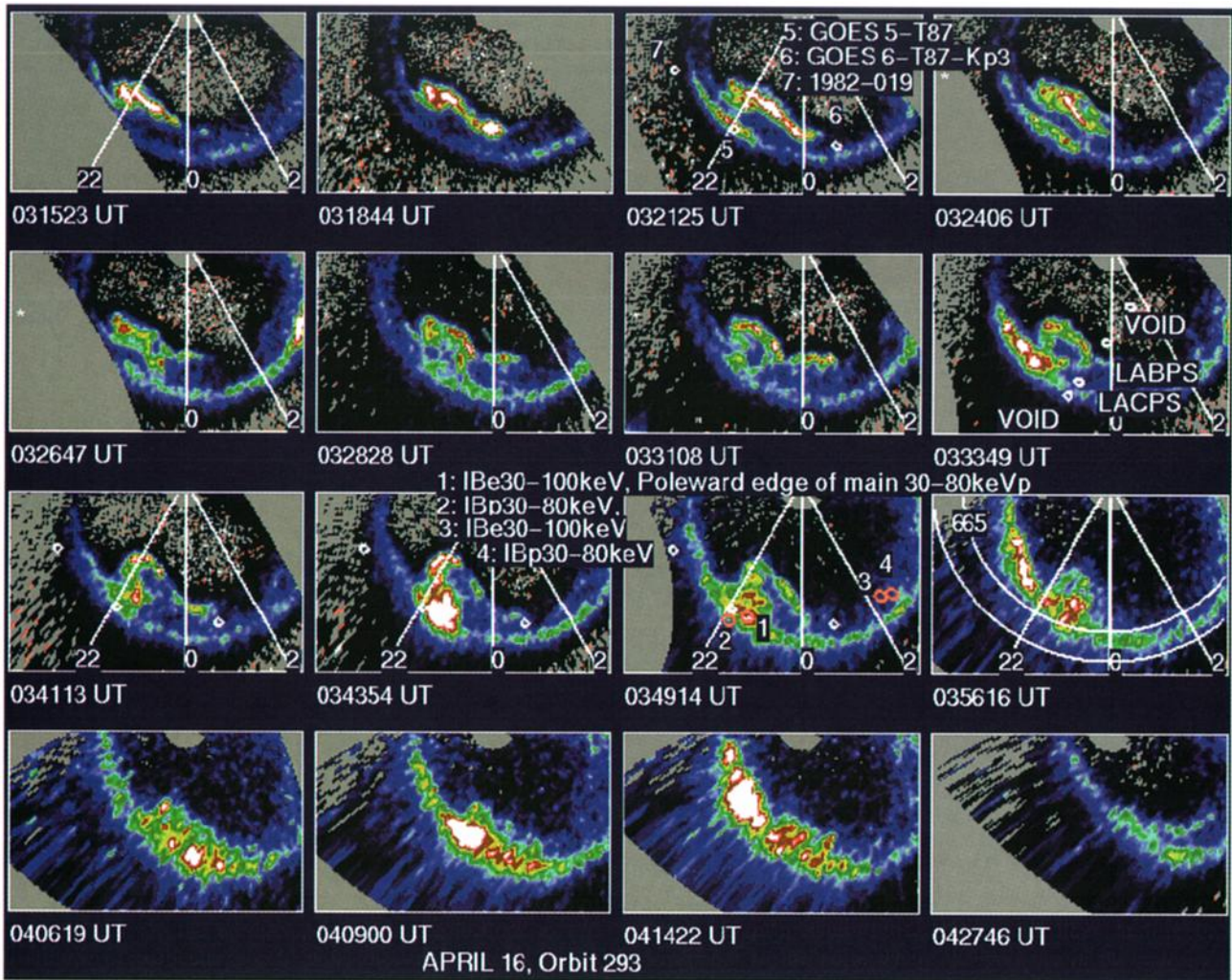


Plate 7. Images on April 16, 1986 from 0315:23 to 0427:46 UT showing 5 auroral intensifications which lead to substorm onset. 22, 0 and 2 MLT are shown as well the projections of low- and high-altitude satellites. The large red circles represent the NOAA 6 IB boundaries for 80-250 keV protons (points 2 and 4 at 0349:14 UT) and 30-100keV electrons (points 1 and 3). The T87 projections of GOES 6, GOES 5 and 1982-019 (from left to right) are shown as the white circles (points 5, 6, and 7). The small white dots in the last panel in the second row show boundaries based on DMSP-F7 particle observations.

has a rather unique conjunction of satellite data with the auroral imagery. GOES 5 was located in the local time sector of four of these multiple intensifications, GOES 6 was further to the west, and 1982-019 to the east. The projections of these satellites to the ionosphere (T87) is shown by the small white circles near 19, 22, and 1 MLT in Plate 7 (see the panel at 0319:04 UT for identification). The errors associated with using the T87 versus T89 model are less than 1 deg Mlat for these projections. Also shown in the third panel of the third row in Plate 7 are the northern hemisphere projections to 120 km altitude of particular points along the satellite track of the Tiros NOAA 6 satellite (large red circles). The various points are labeled in the panel at 0346:33 UT and the legend for these points is shown in the left of that panel. Between 0326 and 0332 UT DMSP-F7 had an overflight near 23 MLT. Particle boundaries based on a neural network [Newell *et al.*, 1991] are shown in the last panel of the second row (0331:08 UT).

The NOAA-6 observations occurred between 0349 (morning sector traversal) and 0357 UT (evening traversal) and allow the

calculation of the isotropic boundaries (IB) for three separate ranges of energetic protons. These points correspond to the poleward boundary of the region where the perpendicular flux exceeds the parallel flux of particles at 800 km altitude. The IB location for the 100 keV electrons (point 1 in Plate 7) also corresponds in this case to where the 30 to 80 keV precipitating proton flux has dropped by a factor of 10 from its peak value. The 80 to 250 keV proton fluxes also drop off near this point (see Plate 8 below). In the magnetotail this should coincide with a sharp transition to taillike field lines and probably corresponds to the point where the pressure in the magnetotail undergoes a rapid change. This location is near the peak in the main UV auroral oval in the evening sector where the auroral activations occurred.

The 30 to 80 keV proton IB and the 100 keV electron IB lie poleward of the main UV oval in the morning (point 4). In the evening the 30 to 80 keV IB (point 2) is approximately coincident with the equatorward edge of the main UV oval and is equatorward of the onset or activation location. This asym-

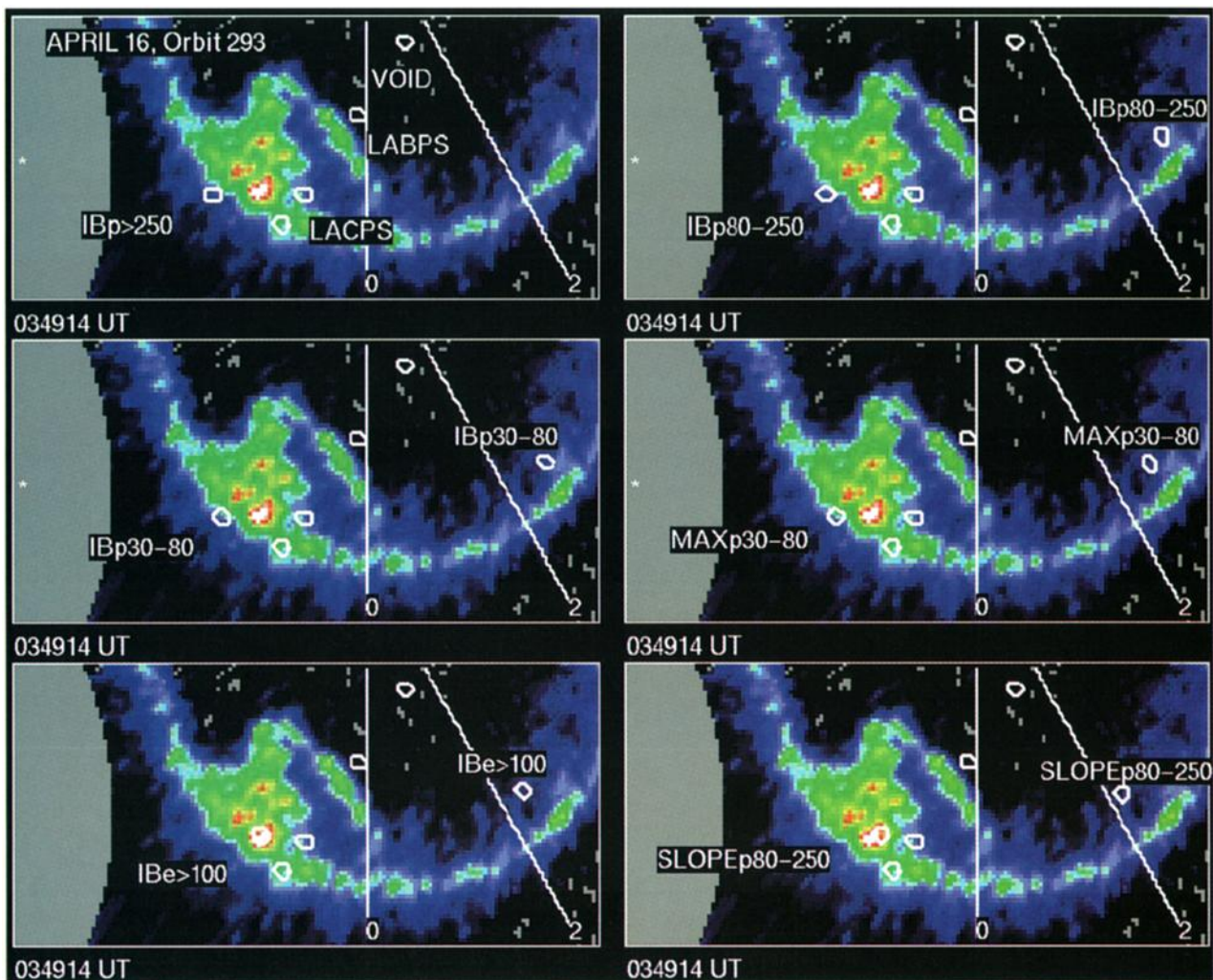


Plate 8. A closeup view of one image taken at 0349:14 UT from the event in Plate 7. The DMSP particle boundaries are shown in each frame near midnight. As well various NOAA-6 boundaries have been labeled in each panel. The following energetic particle boundaries are shown: (upper left) > 250 keV proton isotropic boundary; (upper right) 80 to 250 keV proton isotropic boundary; (middle left) 30 to 80 keV proton isotropic boundary; (middle right) peak in the 30 to 80 keV proton precipitation; (bottom left) > 100 keV electron isotropic boundary; (bottom right) location where the 80 to 250 keV proton fluxes change abruptly. The onset region is associated with the LACPS particle signature and with energetic proton precipitation. (middle right panel). It is approximately coincident with the energetic electron isotropic boundary (in the lower left panel denoted by $IBe > 100$) and lies equatorward of the point at which the energetic proton precipitation changes drastically ($SLOPEp80-250$). This latter boundary is probably related to the location where dramatic pressure changes occur in the magnetotail.

metry between the morning and evening sectors illustrates what appears to be a fundamental difference in the magnetospheric source locations for the main UV oval. This may be related to the difference sense of region 1 and 2 field-aligned currents between these sectors.

The 100-keV electron IB location is approximately coincident with the main UV oval and the site of auroral activation. It should be noted, however, that there was a secondary peak in precipitating 30- to 100-keV electrons coinciding with the energetic proton (30 to 80 keV) peak flux. At lower auroral-type energies the main UV oval and onset location coincides with the LACPS region with the more poleward oval being LABPS precipitation (see the DMSP trajectory). The average energy of the LACPS region just east of onset was 1.8 keV for the electrons and 9.2 keV for the ions.

Plate 8 shows the location relative to the auroral distribution of some of the additional energetic boundaries associated with this event. Table 3 shows the locations of these boundaries projected to 120 km altitude in the northern hemisphere using both the T87 and the T89 magnetospheric models (Kp 3). Also shown are the projections of these points to the equatorial plane of the magnetosphere. Table 3 shows that the higher-energy protons become trapped equatorward of the lower-energy ones and that the energetic electrons are trapped significantly poleward of any of the proton IB locations. The mapping to the Earth's equatorial plane is dependent on which model is used. The T89 model generally places the points tailward and more towards the fwflanks than does the T87 model. The peak proton precipitation (30 to 80 keV) and all of the IB proton locations occur earthward of $x_{GSM} = -7.5 R_E$ independent of the

Table 3. NOAA 6 Energetic Particle Boundaries

Boundary	Energy Range (keV)	Particle Type	CGM 80		T87		T89	
			Mlat	Mlt	xGSM	yGSM	xGSM	yGSM
<i>Morning</i>								
IB	>250	p	undefined	-	-	-	-	-
IB	80-250	p	65.6	2.74	-5.4	-4.7	-6.5	-5.7
IB	30-80	p	65.9	2.65	-5.7	-4.7	-7	-5.9
Peak flux	30-80	p	66.0	2.58	-6.0	-4.7	-7.5	-6.0
Slope	80-250	p	66.9	2.21	-7.6	-4.6	-11.6	-7.4
IB	>100	e	66.6	2.36	-6.9	-4.6	-9.7	-6.8
<i>Evening</i>								
IB	>250	p	63.4	22.1	-5.0	2.4	-5.6	2.6
IB	80-250	p	63.5	22.1	-5.1	2.3	-5.7	2.6
IB	30-80	p	63.8	22.2	-5.3	2.3	-6.0	2.6
Peak flux	30-80	p	63.9	22.2	-5.4	2.3	-6.1	2.6
Slope	80-250	p	65.8	22.7	-6.6	1.9	-9.7	2.7
IB	>100	e	65.4	22.6	-7.0	2.0	-8.3	2.6

p, proton; e, electron.

model employed. The IB electron boundary in the evening sector is mapped to between $x_{\text{GSM}} = -7.0$ and $-8.3 R_E$. This indicates that the auroral activation and the main UV oval near substorm onset appears to be mapping earthward of the point at which the mapping to the magnetosphere becomes very unreliable. The region of rapidly changing proton fluxes is somewhat more variable indicating it is in a region heavily influenced by the strength and configuration of the cross-tail current.

Sergeev *et al.* [1983] showed that pitch angle scattering of particles with a rigidity G in a stretched field configuration (with radius of curvature R_C) would occur such that the loss cone of these particles would be filled when κ was less than about 6 to 8 ($\kappa = R_C/G$). For κ values less than this one would therefore expect to see similar perpendicular and parallel fluxes. This method for predicting the IB proton location has recently been tested and found to be reasonably successful [Sergeev *et al.*, 1993]. The auroral activations therefore are occurring poleward of this $\kappa = 8$ proton boundary. It should be noted, however, that this condition for pitch angle scattering is a steady state one and that time variations can also affect the breakdown of adiabaticity.

The observation that the 80- to 250-keV proton fluxes decrease markedly at about or just poleward of the > 100-keV electron IB location is consistent with an abrupt transition from dipolar and ring current populations to a much more taillike configuration associated with the cross tail current. This occurs just poleward of the auroral activation (see Plate 8) and eastward of the projection of the GOES 5 spacecraft (the white point labeled 5 in Plate 7). The implication of the above observations is that the peak in the main UV oval in the evening sector where onset is occurring is equatorward of this transition region. The observations from the GOES 5 satellite further confirm this suggestion.

GOES 5 was located in the same local time sector as NOAA 6. The T89 model can reproduce the ionospheric location of the proton IB using a slightly stretched Kp 3 model (by increasing the tail current by a factor of 1.19) or a slightly dipolarized $Kp = 4$ model (by decreasing the tail current by a factor of 0.89). The matching is performed assuming that the IB location is

governed by the amount of pitch angle scattering in a stretched field configuration. This matching implies that the field inclination near the IB equatorial location was properly reproduced using these models. The ionospheric proton IB location was embedded with the LACPS precipitation region and lay closer to its equatorward edge. This implies that some of the LACPS precipitation was occurring on dipolar like field lines. The IB boundary of 30- to 100-keV electrons on the other hand occurred in the center of the LACPS precipitation, the main UV oval and the location of the auroral activations.

The variations of the magnetic field at both GOES 5 and 6 are shown in Figure 6. The components shown are H_N , H_E , H_P , and H_{total} which correspond to eastward, earthward, parallel and total fields respectively. On the right side of the figure the data from GOES 5 is presented and vertical lines have been drawn at 0319, 0340, 0406 and 0430 UT corresponding to four of the auroral activations noted above. The last three of these events show a clear stretching followed by a dipolarization of the field at the time of the auroral activations. (The stretching is indicated by a decrease in H_P and an increase in H_E while the reverse holds for the dipolarization). The first event shows a less clear dipolarization.

It is interesting to note that the dipolarization was very abrupt for the 0340 UT event but H_N (eastward) began to change significantly before this time. The parallel component began to increase at 0342:20 UT, and the earthward component began to decrease at 0341:55 UT, but the eastward component began to change a full minute earlier at 0340:21 UT. This component for both the 0340 and 0406 UT events first showed an impulse increase in magnitude by about 20 nT which was then followed by an exponential decay lasting about the 20 min until the next event. The decay time of this impulse was about 20 min (i.e., the time for the field to fall off to e^{-1} of the initial impulse). The dipolarization was finished in about 5 min after which the field underwent a new period of stretching.

It is also noteworthy that the total field was increasing over this interval and that the parallel component of the field was significantly greater for the event at 0406 UT and for the main onset at 0430 UT than at the second event at 0340 UT. The

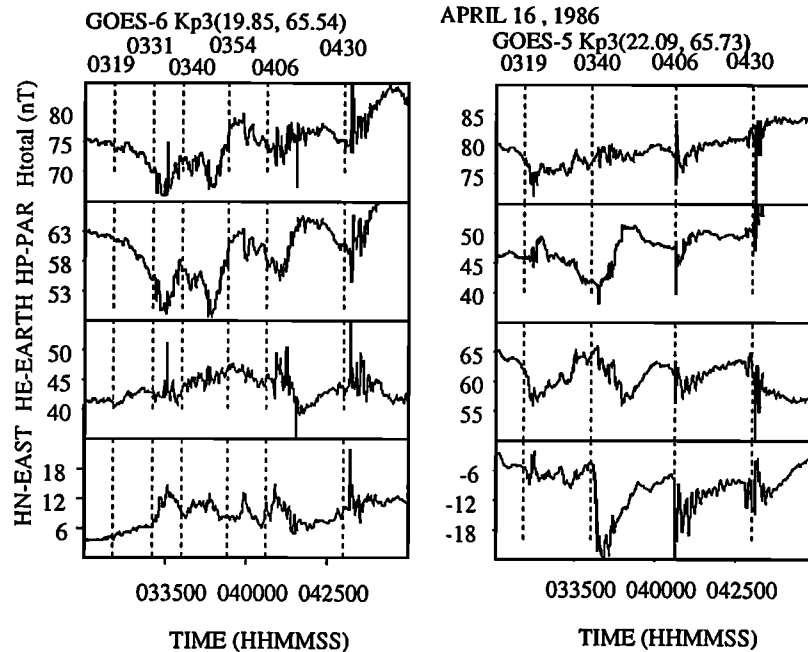


Figure 6. GOES 5 and 6 magnetic field observations for the April 16, 1986 event. The vertical lines show when auroral intensifications were seen in Plate 5. In this case dipolarizations and Pi 2 activity were clearly seen at GOES 5. Later intensifications occurred in a more dipolar configuration than did the earlier ones.

earthward component was also in slightly more dipolar configuration. Thus this multiple activation event showed a series of stretching and dipolarizations, some of which occurred during an IMF B_z northward period. Each activation returned the magnetic field to a slightly less stretched configuration. The main optical onset then occurred in this more dipolar configuration. It is possible that GOES 5 moved out of the active region during the previous activations so the field at that location did not become as stretched. If this were the case then the active region would have to be quite small or the satellite was initially positioned very close to the edge of the active area.

The three events at 0342, 0406, and 0430 UT also showed Pi 2 activity (predominantly in the azimuthal direction). A particularly clear example of this occurred at 0406 UT. During the period of decay in the eastward impulse, this component (H_N) also showed pulsations. The H_E component also showed smaller fluctuations such that the net amplitude was about 24 nT from peak to peak. The logarithmic decrement (i.e., the reciprocal of the number of cycles of the wave before its amplitude had decreased by $1/e$) associated with these pulsations was between 0.4 and 0.65 (the larger value occurring at the beginning of the interval). The wave was elliptically polarized and oriented just off of the azimuthal direction in the antisunward and duskward direction. It remained this way throughout the time interval. It began as a left-handed polarized wave but this changed such that by 0412 UT the wave was right-handed.

This change in polarization could occur if pairs of field-aligned currents propagated over the satellite. This would require that the satellite lay tailward of the onset region and that the pairs moved eastward relative to the satellite. This is consistent with the westward impulse in the field being associated with an upward field-aligned current earthward of the spacecraft.

Another alternative is that the satellite lay earthward of the wave which propagated westward. This gives the left-handed

sense at the start of the interval. If the electric field increased during the next few minutes, then although the wave was still propagating westward in the plasma frame of reference, observations in the satellite frame of reference could reverse polarity. This explanation was used by *Takahashi et al.* [1987] to explain some Pc 5 wave observations.

Another natural explanation is one put forth by *Hopcraft and Smith* [1986a, b]. In their model the Pi 2 is related to reconnection which generates normal mode oscillations of the neutral sheet occurring tailward of the spacecraft. These couple to standing waves in the near-Earth region. For this scenario to work, the reconnection site needs to be to the west of the satellite (consistent with the auroral observations). The sheet would have to move such that the satellite at later times was found at higher distances from the neutral sheet. This would then account for both the direction of the major axis of polarization, and the change in polarization. This is also consistent with the auroral observations which show a coupling between the high-latitude oval and the main UV oval.

The observation that the H_N impulse occurred about 1 min before the dipolarization (the 0340 UT event) would be consistent with Alfvén transit times necessary to establish current closure with the ionosphere. This points to a magnetospheric source associated with the field aligned current and to a mechanism for this initial current which is unrelated to a cross-tail current diversion. This would require a precursor electric field variation in association with the field-aligned current prior to the dipolarization. Another possible explanation for this delay might be that the spacecraft is at first outside of the current wedge and is initially only registering the signature of the field-aligned current system. A third possibility might be that the changes to the H_N component are associated with a flux rope which has the same orientation as the IMF B_y . It should be noted however that this would imply a factor of 5 increase between the IMF and geosynchronous orbit. Also

since GOES 6 (see below) saw smaller variations in the opposite direction this possibility does not seem likely.

The exponential decay of the Pi 2 oscillation with a logarithmic decrement between 0.4 and 0.65 and a period of about 2 min is consistent with an Alfvén wave bouncing between ionospheres until equilibrium is reached [Goertz and Boswell, 1979]. Sonograms performed on the GOES data showed several harmonics associated with Pi 2.

The magnetic field data from the GOES 6 satellite is shown on the left side of Figure 6. Additional time lines have been drawn at 0331 and 0354 UT since other activations were seen at these times near this magnetic local time. As one might expect from the two satellite locations relative to the activations, the signatures at GOES 6 were less clear, and the timing of the dipolarizations not as good as with GOES 5. In general, the H_N component responded oppositely at the two satellites, that is, positive at GOES 6 and negative at GOES 5. As well it is interesting that the events at 0331 and 0340 UT appear quite differently at the two locations. There was nearly no signature at GOES 5 of the 0331 UT event, whereas a dipolarization occurred at GOES 6. During the second event, when GOES 5 showed a dipolarization of the field, the GOES 6 field was becoming more stretched. This indicates, consistent with the auroral observations, that these activations were local in nature and show that while one portion of the magnetosphere was relaxing the other was apparently storing energy.

The Los Alamos satellite 1982-019 (point 7 in Plate 7) also registered energetic electron flux changes associated with each of these activations. These are shown in Figure 7. The dashed vertical lines in Figure 7 are for the same times shown in Figure 6 and correspond approximately to activations in the aurora. The lowest-energy channels showed 5 distinct flux enhancements which occurred approximately in association with each of the activations at 0319, 0331, 0340, 0406, and 0430 UT. All

of these events were dispersed in energy. The magnitude of each enhancement grew in successive events so that by 0430 UT the change was about an order of magnitude at all energies between 65 and 300 keV.

The first three events show a decrease in the highest-energy fluxes coincident with the lower-energy enhancement. The dispersion in the energy flux indicates that these events are associated with a loss of particles from the drift shell. Such events have been called drifting electron holes [Sergeev *et al.*, 1992]. This could be a result of strong field line curvature. These first events probably represent pseudobreakups or the "micro injections" discussed by Yahnin *et al.* [1990]. If one uses weak injections and the Pi 2 as a definition for substorm onset then each of these minor auroral activations would have to be considered onsets.

Summary. Periodic intensifications of the main UV oval eventually resulted in an optical auroral substorm. One of these precursor events showed AAFs with a mode number of about 20 to 30. These intensifications, which appeared every 20 min or so, could be connected to stepwise changes in the azimuthal angle of the IMF. Another of these events seemed to be triggered by the equatorward drift of an auroral streamer which broke off from the most poleward oval and drifted down to the main UV oval at which time the AAF developed. These events would each be considered an onset if injections, dipolarizations, and Pi 2 activity at geosynchronous orbit were used as the defining characteristic.

Geosynchronous orbit and low-altitude satellites were very well positioned to check mapping and to determine the locations of onset relative to the energetic ion boundaries. In this case, onset appeared to originate on the main UV oval, equatorward of geosynchronous orbit, near the 30- to 100-keV isotropic electron boundary (IB), and equatorward of the location where the 30-250 keV ion flux began to sharply decrease. This

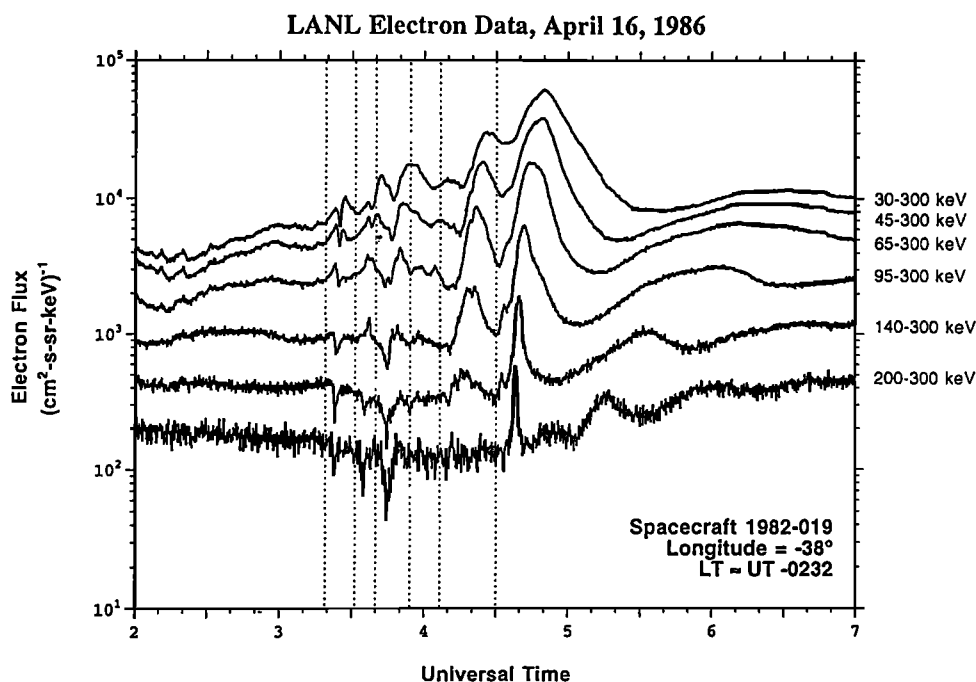


Figure 7. Energetic particle flux observations for the event shown in Plate 7 as recorded at the satellite 1982-019. The dashed vertical lines are at 0319, 0331, 0340, 0354, 0406, and 0430 UT. Dispersed injections were seen in association with each of the auroral activations (see text).

then puts the onset at the poleward edge of the ring current particles probably close to where the nightside cross-tail current peaks.

The DMSP data show that the LACPS particle region changes to a LABPS signature at substorm onset. The GOES satellite data indicated that dipolarizations could be occurring in association with the periodic intensifications and that these could be localized such that one sector could be in a "growth phase" condition while another sector could be dipolarizing. Observations of one magnetospheric location showing dipolarization, while tail stretching occurs elsewhere have been previously reported by *Singer et al.* [1985]. Localized growth phase signatures prior to a major onset have also been noted elsewhere [*Reeves et al.*, 1993a].

The event in Plate 7 also showed that the main onset could occur in a more dipolar configuration than during the previous minor events. This supports a view in which the onset mechanism is not strictly related to the degree of field stretching at geosynchronous orbit. Energetic particle injections were seen many hours in local time away from these pseudobreakups indicating that these small activations can be important on a larger scale in the magnetosphere.

Multiple injection substorms have previously been studied by *Reeves et al.* [1992]. In that study there were three distinct major substorm injections. Those authors found it difficult to account for all of the injections using a near Earth neutral line model. The conclusion was that there must be two separate acceleration regions, one near geosynchronous orbit and the other in the tail. In the case studied here each optical substorm onset had a very short duration, was localized in nature and occurred well equatorward of the open-closed field line boundary. This supports the idea that geosynchronous substorm signatures can occur independently of reconnection in the tail [*Kennel*, 1992; *Reeves et al.*, 1993b].

One of the intensifications shown in Plate 7 (0331 UT) suggests that events near the open-closed field line boundary can propagate inward to the inner portion of the central plasma sheet and trigger AAFs. The generation of these auroral streamers may be related to reconnection. Two arc systems "splitting" near the poleward boundary of the auroral zone was predicted as a signature of reconnection by *Atkinson* [1992]. With enhanced flow due to localized reconnection one might then expect an association between these streamer-AAF onset events and the bursty bulk flow events described by *Angelopoulos et al.* [1992]. In the inner magnetosphere the associated signature of an auroral streamer/AAF event appears to be a drifting electron hole.

If one uses the high-altitude data to define when an onset has occurred then one would conclude that each of these minor auroral activations was a substorm onset or at the very least a pseudobreakup. This event showed that near-Earth onsets or activations can be driven by more distant tail processes as suggested by *Baker et al.* [1993] but also shows that a major substorm can only occur when conditions are appropriate in the ionosphere and the near Earth region. This can sometimes take a number of separate events which eventually provide conditions appropriate for a major one.

3. Statistics of AAF Onsets

A detailed study of substorm onsets over the time period from July 17 to July 29, 1986, was undertaken. This consisted of 36 substorm onset events of which 27 showed AAFs within

a few minutes of substorm onset (depending on the definition chosen this could be before or after onset). These tended to originate before the poleward motion of the aurora began. Sixteen examples of AAFs near substorm onset are shown in Plate 9. In these cases there are typically two or three activations which occurred within a region of brightening which extended about one hour in local time. Some of these occurred during quiet intervals while others appeared on the main UV oval during a double oval configuration (i.e., recovery phase of a previous substorm).

Using an expanded data set covering the Viking observing period, 80 substorm onsets were identified. The average magnetic coordinates of these onsets was 65.9 ± 3.5 CGMlat with range from 56.2 to 73.1 and an average CGM local time of 22.9 ± 1.2 . The average *Kp* value at the time of these onsets was 2+. For onsets with AAFs (this study was limited to the July period mentioned above) the mean local time remained the same but the latitude shifted equatorward to 63.8 ± 3.3 Mlat with a range from 56.2 to 69.6. In the set of 80 onsets, 17 of these were found to occur on the main UV oval during a double oval configuration (i.e., deeply embedded within the closed field line region). The average magnetic latitude of these double oval onsets (64.7 Mlat) was more consistent with the AAF type of onset. The large errors associated with these averages is at least partially due to the limited time resolution of the imager (1-s resolution repeated every 20 or 60 s). An onset can expand significantly in 60 s. The locations selected were generally the location of the peak intensity.

In order to understand the state of the magnetosphere during these events, 1 hour averages of the solar wind conditions were taken associated with the AAF onsets. The average solar wind density was 17.4 cm^{-3} with a solar wind speed of 409 km/s. The resulting solar wind pressure (4.8 nPa) was quite high for these events indicating that solar wind pressure has some influence on AAF onsets. The average variance in IMF B_z was also high in comparison with the variance in the other components indicating changes in IMF B_z also plays a role (consistent with the individual examples shown above).

Figure 8 summarizes results of investigating the azimuthal "wavelength" of the onsets for 27 AAFs. A total of 115 measurements were taken and a histogram was constructed. The wavelengths were measured directly on the original digital data by associating each pixel on the image with a location above the Earth (assuming an altitude of 120 km). The wavelength was taken as the distance (along a great circle route) between the peak intensity in successive intensifications. The error associated with these observations varies depending on the altitude of the Viking spacecraft. The AAFs for this portion of the study were measured only for the image closest to the explosive onset and so reflect values associated specifically with the onset process. The measurements show that AAFs range in wavelength from about 130 to 600 km with an average of 307 ± 115 km. It is important to note, however, that the distribution of the wavelengths is strongly skewed toward smaller values with the most likely value being about 170 to 210 km. There appears to be a sharp cutoff near 130 km (a mode number of about 135). This cutoff is probably not due to an instrumental limitation since wavelengths down to 75 km could be accurately identified using Viking data. This could possibly be a subjective cutoff in that smaller-scale events were not noticed when the wavelengths were selected and measured. If this is a real cutoff then this result implies the onset mechanism can be associated with small magnetos-

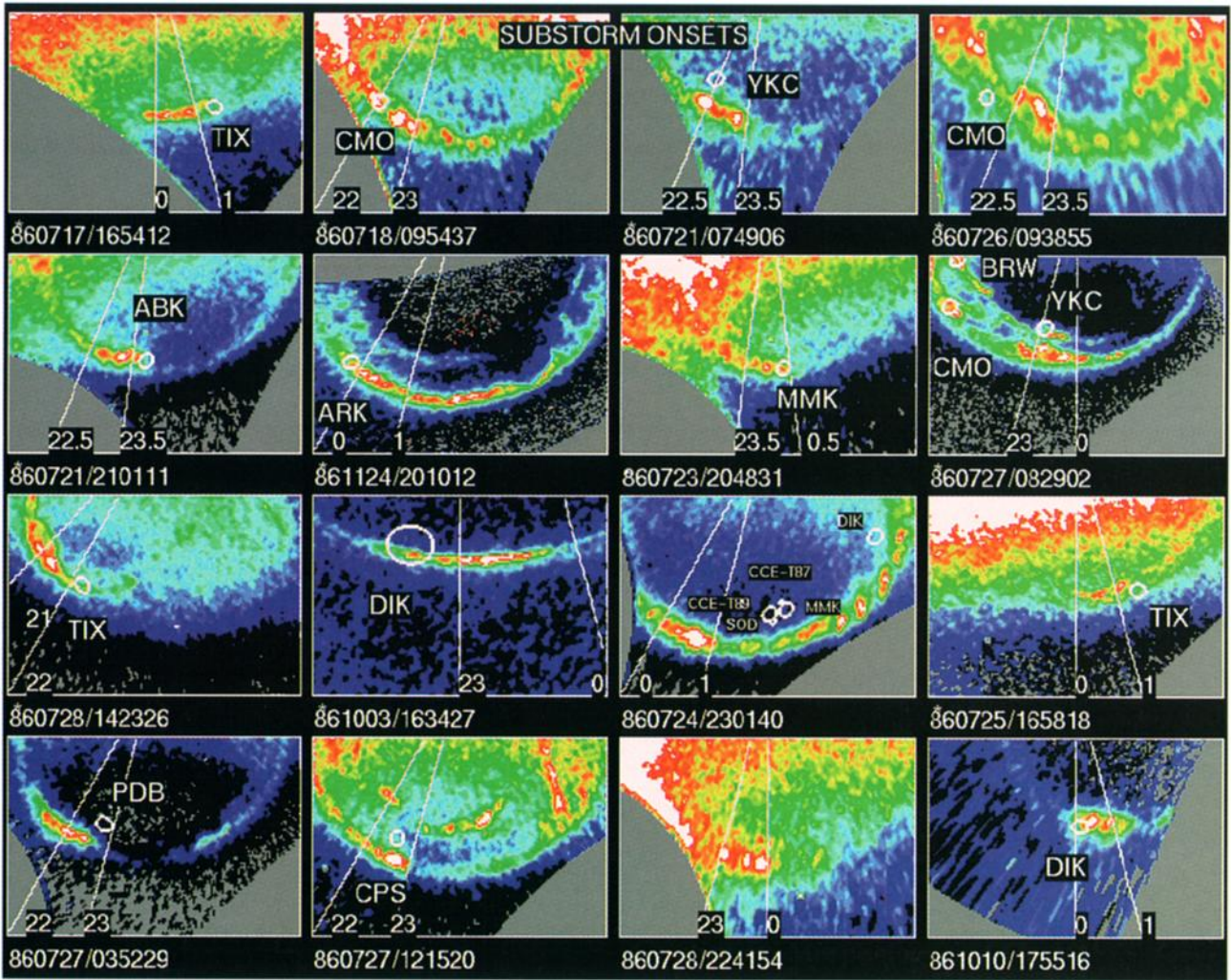


Plate 9. Examples of AAFs near the time of optical substorm onset. Typically the active auroral region is about 1 hour in local time extent although the AAFs can cover a broader region of local time.

pheric azimuthal wavelengths down to some cutoff value. A mode number of 135 converts to a scale size of $2\pi L R_E / 135 \approx 0.05L R_E$ in the magnetosphere.

It should be noted that the AAF events discussed in this paper should not be confused with vortex streets seen elsewhere on the auroral distribution as reported by *Murphree and Elphin-*

stone [1988] and *Murphree et al.* [1994]. In these events, small-scale spirals form on the poleward edge of the auroral distribution usually late in the substorm expansion phase. These are probably due to magnetic shear associated with upward field-aligned current perturbations [*Hallinan*, 1976]. AAFs considered here are specifically the features which appear in the time period near substorm onset on the main UV oval. These AAFs do not always take the form of auroral spirals. The accompanying signatures both on the ground and at high altitude differ from these small-scale spirals. Whether or not they bear more than a superficial resemblance to other kinds of vortex streets remains to be seen.

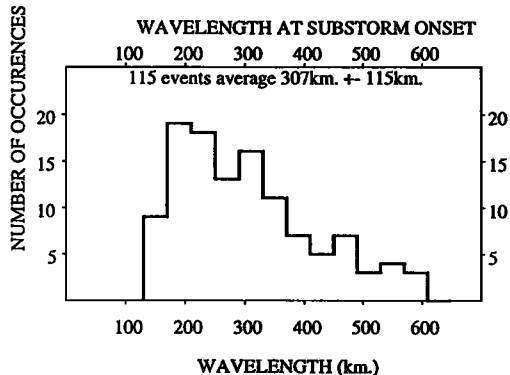


Figure 8. Occurrence rate of the spatial scale associated with AAFs prior to substorm onset.

4. Substorm Morphology and Onsets

In the above cases, it is clear that the form a particular substorm intensification and/or onset takes is strongly dependent on previous conditions. These cases are not unusual events but they do not fit obviously into the morphology of a full substorm as described by *Akasofu* [1964]. *McPherron* [1979] has described in some detail the magnetospheric substorm, substorm sequences and multiple onset substorms. In that article, it is

noted that conflicting views exist as to what is or is not a substorm. Are weak events that do not develop beyond some threshold in amplitude and spatial extent to be considered "pseudobreakups"? Are there two different types of substorm onset, one local and the other the more familiar global event? Are events which bear little resemblance to one another to be grouped together under the single heading of "substorm"? It seems that as time goes by there appears to be an ever growing grey area concerning what constitutes a substorm.

More recent articles describe pseudobreakups as having signatures which one normally associates with a full auroral substorm onset [e.g., Koskinen *et al.*, 1992; Ohtani *et al.*, 1993]. What distinguishes these events from the others? In the past the existence of a growth phase of an auroral substorm was criticized on the grounds that one could not be sure of an exact onset time based on incomplete information and that this phase was defined based on whether or not a substorm expansive phase subsequently occurred. The same problem, however, appears with regard to the substorm onset itself. Substorm "onsets" can occur at any phase of an auroral substorm. They are distinguished from pseudobreakups based on whether or not a global substorm occurs and sometimes by whether they are the first event or not. A similar semantic difficulty exists with respect to the WTS. Traditionally, this form is associated only with the spiral form which exists at the west tip of an expanding auroral bulge. This same form however can be found at nearly any local time, at any location relative to the substorm bulge and at any time during the substorm. Is this form also to be defined by what it accompanies rather than by its own intrinsic characteristics?

The first event in this paper showed an onset which was preceded by AAFs. The first "expansive" phase lasted only 10 min (from 2032 to 2042 UT in Plate 1). This was followed by the fading of the auroral bulge and equatorward motion.

This lasted only 5 min after which a new intensification occurred which lasted another 15 min. In this case, the expansive phase based on the AL index lasted 30 min but based on a strict definition, there was an expansion, recovery and new optical onset within this 30-min time span. The time at which substorm recovery occurs is in general also very difficult to define optically. Locally, it can be defined as when the aurora in a particular local time sector ends its poleward progression. Globally, however, arc systems which define the boundary of the double auroral oval can continue to move poleward (at local times away from midnight) long after all activity has faded.

New activations within the double oval configuration also create a problem for terminology (see Plates 5 and 7). They appear during the recovery phase of a previous substorm and so are not the events which Pytte *et al.* [1976] refer to as multiple onset substorms. They more closely resemble events observed by Kamide *et al.* [1977]. They repeat every 10 to 20 min, last only a few minutes and yet by some criteria would be considered to be substorm onsets. On the other hand, they have no resemblance to what is commonly thought of as a global optical auroral substorm. In these cases, high-altitude data would give a clear interpretation that these events were substorm onsets. Ionospheric researchers, however, would probably disagree. This is further complicated by other events as described below.

The AAF type of substorm onset is not the only form of onset which can occur. This is illustrated in Figure 9. The top panels of Figure 9a show the AAF type of onset. Azimuthally spaced auroral forms with a mode number of between 30 to 135 occur near the peak in the main UV oval. They propagate eastward in the morning and have magnetic pulsations in the Pc 5 period range associated with them. The AAF furthest to the west is more likely to develop into an explosive substorm bulge. As indicated by the bottom panels of Figure 9a, there is a different type of onset which begins in the west and pro-

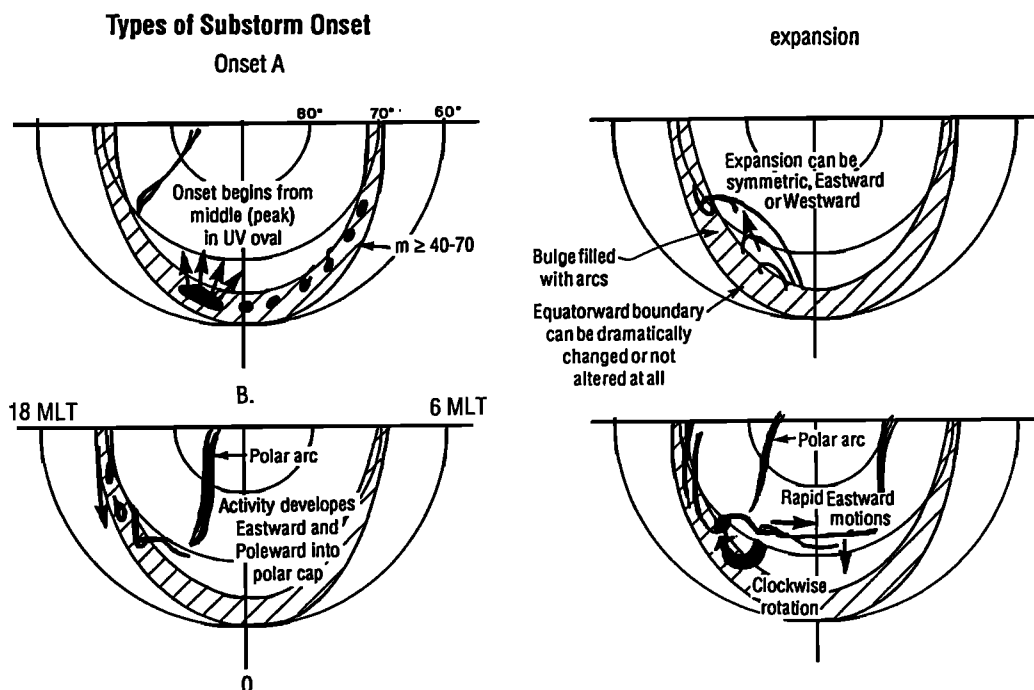


Figure 9a. A modular view of substorm morphology. Schematic of two types of substorm onset. The top panels illustrate the type studied in this paper. The bottom panel shows a type of event which may be related to PSBL processes or to reconnection at the distant neutral line.

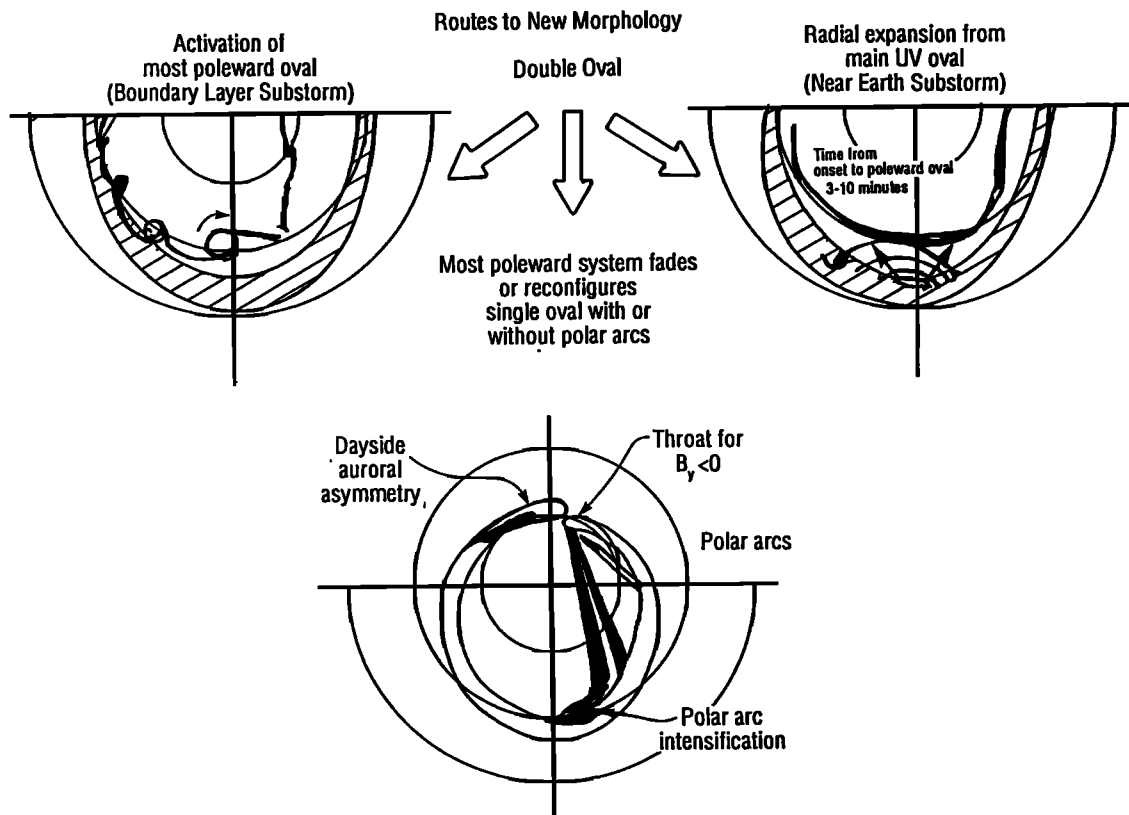


Figure 9b. A modular view of substorm morphology. Schematic of three routes the auroral distribution can follow in substorm recovery phase illustrated the two fundamentally different regions which can activate.

pagates toward the east at speeds greater than 5 km/s. In this local time sector, polar arcs (which may be related to processes in the distant tail low-latitude boundary layer) connect to the nightside poleward auroral zone (which is probably linked to the plasma sheet boundary layer) where these onsets begin (see Plate 6 in *Elphinstone et al.* [1991a]). These types of intensifications can occur at virtually any time during the substorm process, similar to what is observed with the AAF onsets.

The conflicts mentioned above can be partially resolved by considering the substorm to a composite event consisting of many different modular elements. Pseudobreakups can be viewed as single modules which do not combine with others to produce a more global event resembling the *Akasofu* [1964] view. Growth phase can be thought of as an independent system which may influence subsequent activity. Auroral spirals are signatures of upward field-aligned current perturbations. When and where they occur can tell you how the system is reacting to external and/or internal influences. Any particular substorm can then be envisioned to be a composite of modules fit together in parallel or in series in such a way as to reproduce the observations. This can be thought of as a technique for "building your own substorm." Each module could be viewed as an independent process which can be studied in its own right. When some of these elements interact then the coupling process can be studied and the interdependencies of the modules outlined. In this manner one might determine that substorm onsets and pseudobreakups are essentially identical but that they evolve differently due to coupling to other substorm elements (such as growth phase elements or ionospheric influences). This modular view emphasizes that different

regions of the magnetotail can be active independently of each other as well as interacting together. The form a particular substorm takes is then determined by preconditioning in all regions of the magnetosphere and thus the time history of a given event is fundamental to its interpretation.

The large-scale auroral distribution during active conditions can be divided into two important configurations which are distinguished by whether a double oval exists or not. Further, two separate types of activation can occur. If the double oval has not formed then the two types of activations resemble the configurations shown in Figure 9a. If, however, the double oval does exist then the two types of intensifications correspond to two distinctive regions which activate. If the poleward set of arcs activate then the "route" which is followed is schematically illustrated by the left side of Figure 9b. An event of this type which occurs as the plasma sheet thickens is shown by *Cogger and Elphinstone* [1992]. The dynamics of the activation frequently (but not always) take the form shown in the bottom panel of Figure 9a. Similarly if the more equatorward set of arcs activate (right side of Figure 9b) then this frequently (but not always) results in an AAF type of onset (bottom panel of Figure 9a). These more equatorward events comprise about 20% of the onsets recorded by the Viking spacecraft. They have been used in many Viking substorm papers to support a near Earth source for substorm onset [e.g., *Elphinstone et al.*, 1991a; *Murphree et al.*, 1991].

Figure 9b shows the importance of the double oval configuration in understanding the the various types of activations. If a double oval did not exist, then it would be difficult to say much about where these activations map to in the magneto-

sphere. When it does, however, then the activations can occur simultaneously or separately and they can be related to completely different ionospheric/magnetospheric regions. These activations are examples of modules which can clearly be related to different magnetospheric regimes and hence also different physical processes.

The modular view of the substorm allows for each portion of the standard picture to occur or not occur dependent on preconditioning. It also allows for additional components such as a growth phase. A growth phase may or may not be followed by an arc intensifying. The onset may or may not (a pseudobreakup in the old terminology) be followed by an substorm bulge which, in turn, may or may not be followed by a traversing arc which brightens near the end of the poleward motion. This may or may not develop into a larger-scale configuration which spans most local times. On the other hand, the most poleward system may activate without a preexisting substorm bulge. This indicates that each of these events is probably linked to separate physical processes (although coupling usually exists). For instance, the development of the global configurational change is probably related to the disturbance of boundary layers in the magnetosphere and the refilling of the plasma sheet during conditions of plasma sheet recovery. If one built a picture of a developing substorm, the picture could be modified at virtually any time in its development to incorporate a new set of one or more of these modules. This scheme of development is not part of the standard picture.

As well as these more general fundamental modules, however, there is a secondary set of events which can also presumably be linked to distinct and potentially independent processes. In a given substorm event, features such as omega bands may or not develop. For these type of events the time at which they occur is dependent on when the physical process governing them is active in the ionosphere/magnetosphere. They can develop while a substorm bulge is occurring (expansion phase in the standard picture) or after the double oval has formed. Similar statements can be made about auroral streamers and auroral pulsations. Since this occurs observationally we know that the physical process associated with these features is not confined to a particular time in the substorm process (as in the standard scheme). These events which are less fundamental (to the morphology at least) might be termed secondary modular elements. The only apparent restriction for when these events occur is that there must have been an explosive onset previously (potentially hours before).

This new view of an auroral substorm could help resolve competing theories of the substorm process. *Lui* [1991] came up with a synthesis to describe the magnetospheric substorm. He did this assuming that the global process always took place. Using the modular view of a substorm however, different regions of the magnetosphere could be sources for auroral brightenings dependent on their preconditioning. On occasion, the dayside ionosphere and magnetosphere could be in a state where a disturbance at the magnetopause creates obvious growth phase motions of the aurora and auroral activations which move toward the nightside. This disturbance might eventually trigger onset. On the other hand, conditions in the night sector may not be appropriate and either nothing or only a single other module is activated. In certain circumstances only the near-Earth region might activate with the more distant tail not being triggered or properly preconditioned. In other cases the deep tail could create auroral activations associated with reconnection with the near-Earth region not responding. This might

produce localized activations near the poleward auroral boundary. If both regions activate then the result might be a substorm limited in spatial extent to the night sector. If conditions are right the substorm process could extend to all local times. The module sequences listed above are just a few possible combinations. These features could each trigger others and produce causal relationships between them.

5. Discussion

In this paper a few examples of AAF type auroral substorms were shown. Most of these events were accompanied by ground magnetic pulsation activity in the Pc 5 period range. In this small sample it was demonstrated that when the onset actually occurs and whether in fact it was an onset is strongly governed by the definition used. Both AAFs and coexisting omega bands were observed to propagate eastward before onset. The onsets appear to occur predominantly in the evening sector about 1 hour away from magnetic midnight. The long period pulsations in the evening appear to propagate westward to the west of onset (opposite to the direction in the morning sector).

Some evidence exists that shows AAFs may, on occasion, be driven by processes occurring deeper in the tail (this was seen for two examples in this paper). The AAFs can begin 15 min prior to the explosive poleward motion of the auroras and this latter event can occur several minutes after what would be considered substorm onset based on energetic particle injections at high altitude (the July 24 event). They can occur in association with dayside precursors which propagate toward the nightside.

Activations can occur periodically (every 10 to 20 min) which eventually result in what would be considered to be a large-scale substorm onset. These activations can be quite localized and be associated with AAFs, but they do not necessarily result in large poleward motion. On the other hand, high-altitude satellites could register these events as injection events and as dipolarization events accompanied by Pi 2 activity. The main onset after these activations occur can take place in association with the field at geosynchronous orbit being more dipolar than at the beginning of the interval. It appears then that these multiple activations leading up to a main onset event somehow precondition the region to allow a major onset to occur. Onsets typically occur premidnight and near the most westward extent of the AAFs indicating that there is probably a special significance to the evening sector versus the early morning. This may be related to ionospheric conductivity differences between the two regions.

Onsets which began during the recovery phase of previous substorms originated near the peak in the main UV oval and took several minutes to reach the most poleward set of arc systems in the double oval. This observation indicates that optical substorm onset is not driven directly by the last closed field line reconnecting and shows that this field line can not reconnect for several minutes (up to about 10) after onset. This statement assumes that the most poleward arc system exists on closed field lines. The multiple activation events frequently never reach this outer boundary. This indicates that if a near Earth neutral line is involved, reconnection must not continue to the point where flux is released down tail.

These onsets appear to originate within the region 2 field-aligned current system and the associated discrete arcs appear as LABPS signatures deeply embedded within a LACPS system. They seem to occur at the interface between ring current energy proton precipitation and the earthward edge of the cen-

tral plasma sheet. This occurs at the tailward end of the inner edge of the central plasma sheet (i.e., the point at which the higher energy central plasma sheet particles begin to disappear leaving only particles of lower energies and the higher-energy trapped ring current particles). All of these observations support the mapping of the main UV auroral oval put forth by *Elphinstone et al.* [1991b]. The double oval onsets also tend to occur during storm times indicating that there may be a preference for these forms to exist during active ring current conditions. Another significant observation is that the region which contains these AAFs and which eventually results in an explosive poleward motion is typically about 1 hour of local time in extent. This tends to imply that the onset mechanism is linked to a large-scale magnetospheric process.

There are relatively few onset mechanisms which deal with azimuthal wavelike forms which can exist during or prior to substorm onset. Cavity mode resonances have much smaller mode numbers and so are not viable in explaining the observations in this paper. Although the boundary layer model of *Rostoker and Eastman* [1987] does involve wavelike forms, the AAF events in this paper clearly originate from much closer to the Earth than the PSBL and are unlikely to be associated with a low-latitude boundary layer substorm model. Some of the above observations, however, do suggest that AAFs can on occasion be related to activity originating deeper in the tail which propagates earthward. In the near-Earth region this preconditioning somehow triggers an AAF event. Other observations relate them to processes which might go on concurrently with Pc 5 and omega band activity. Conductivity indirectly may play a role and some of these events must be able to occur without reaching the open-closed field line boundary. Further, this type of onset is not the only one to exist. It seems important that existing substorm theories make some attempt to account for the above set of observations.

In the meantime it is informative to determine whether the predictions of any current model agree with the above set of observations. One theory of onset does seem to deserve some special attention. This is related to a modified flute and/or ballooning instability which has been developed by *Ivanov and Pokhotelov* [1987] and *Ivanov et al.* [1990, 1992]. A summary of the relevant features of the modified flute model is given below. Observations by *Roux et al.* [1991a, b] have previously indicated that the ballooning mode could be important. Work by *Ullaland et al.* [1993] also indicated that even a normal ballooning mode could be unstable under the conditions prevailing in a prestorm condition. *Pu et al.* [1992] studying 22 onset events also found evidence for large radial pressure gradients and conditions at GEOS 2 which were favorable to the ballooning instability. These works, however, tested an instability criterion which does not include the stabilizing effects of plasma compressibility. This has been investigated in detail by *Ohtani and Tamao* [1993]. They found that in most of the 22 events even a necessary condition for the instability is not satisfied [see *Ohtani and Tamao*, 1993, Table 1 and Equation (5)]. Thus the stability of the near-Earth magnetotail against the ballooning instability remains controversial.

We suggest in this paper that additional physics must be considered in order to completely evaluate whether or not ballooning is feasible in the near-Earth region. For example, *Chan et al.* [1994] have recently shown that pressure anisotropy can also be quite important and that for observed values of pressure gradients the Alfvén-ballooning mode can be unstable if the ratio of parallel to perpendicular pressure is less than

about 0.5. (For the 22 onsets studied by *Pu et al.* [1992] this ratio was between 0.88 and 1.25. Calculations by *Vetoulis and Chen* [1994] show a strong dependence of the damping of the Alfvén-Ballooning mode with the mode number (their Figure 3). They show that damping due to field line resonances is negligible for $m \approx 100$ and odd symmetry of the resonance about the equator ($n = 1$). There is strong damping, however, when the azimuthal mode number is less than about 30. These results are remarkably consistent with the observations presented here and may indicate the importance of the Alfvén-ballooning mode in the substorm process.

We now consider another possibility for easing the instability requirements. The normal flute instability was initially developed by *Swift* [1967] but requires a high radial pressure gradient which does not normally exist in the inner magnetosphere. *Ivanov et al.* [1987], however, showed that under certain conditions the flute instability could occur under less stringent radial pressure gradients. They found that the introduction of pressure gradients which were not aligned with the curvature vector of the magnetic field could allow growth of the instability. This condition is related to having field-aligned currents flowing to the ionosphere via a $\nabla P \times \nabla V$ term in the magnetosphere (P represents pressure and V the flux volume). This has been developed further by *Ivanov et al.* [1992] to include finite beta conditions and a parallel wavenumber, at which point this instability becomes a ballooning instability.

The above condition implies that the magnetosphere could be unstable to a flute instability if some threshold field-aligned current occurs. *Ivanov et al.* [1987] have called this the flute instability in variable pressure with finite beta. In their model the direction of the wave vector will lie between the ∇P and the ∇V vectors. If there exists a compression of the magnetic field in the midnight sector, then the wave vector associated with the instability is westward in the evening and eastward in the morning. This is equivalent to assuming a current wedge sense to the field-aligned currents in the midnight sector in a region where the pressure gradient is Earthward. Since the $\nabla P \times \nabla V$ term would be zero at midnight, this theory would reduce to the standard model at midnight and would indicate that this region is stable to the flute instability. The observation that substorm onset occurs away from the midnight meridian is consistent with this theory.

The frequency of the wave corresponds to the ion drift frequency and is only unstable for azimuthal wavelengths exceeding the ion gyroradius. Otherwise, the instability works best for small azimuthal wavelengths. This result resembles the histogram results of Figure 8. For comparison with the minimum wavelengths observed, the proton gyroradius in R_E is given by $0.72\sqrt{E}/B_z$, where E is the perpendicular kinetic energy of the proton in kiloelectron volts and B_z is the magnetic field in nanoteslas. In order for the minimum wavelength ($0.05 L$ in R_E) to exceed the proton gyroradius this requires that the energy of the ions be less than $(0.07LB_z)^2$ keV. For a value of B_z of 10 nT this implies an energy of the ions less than 50 keV at $L = 10$ and less than 17 keV for $L = 6$. This result is relatively consistent with the observed wave speed corresponding to the gradient drift speed of 20-keV particles. The combination of the gradient drift speed and minimum wavelength can be used to approximate the minimum period which then becomes $2.87 \times 10^5 / (B_z L^2 \sqrt{E})$. The minimum period using this simple method is 64 s at $L = 10$ and 178 s at $L = 6$. These values are consistent with the observations. One could also expect magnetic and pressure pulsations associated with this instability.

The ideal conditions for growth are short field lines, small perpendicular wavelengths (greater than the ion gyroradius), and a large radius of curvature. *Ivanov et al.* [1992] showed that a decrease in β could at least partly offset the stabilizing effects of a small radius of curvature. As an example, they chose a line current to define a magnetic field configuration and tail field curvature. They found that the radial dependence (r^{-p}) of the pressure must decrease with r faster than when $p = 2\gamma/(1 + \gamma\beta/2)$, where γ is the adiabatic index. The conditions for instability also depend on the ionospheric conductivity. A study could be made in the future to determine under what conditions the instability could grow in more realistic magnetic field topologies and pressure configurations.

If a parallel wavelength is involved then the instability is somewhat more difficult to excite. This would then result in a ballooning mode. *Ivanov et al.* [1992] showed that for values of parameters in the near-Earth region using a dipole configuration this instability could have growth times of the order of a minute. Under high conductivity conditions ballooning of this type requires a long parallel wavelength compared to the natural field line wavelength.

This theory might explain some aspects of the AAFs. It may be that as different criteria for instability are reached, the manifestations in the aurora change. AAFs which develop in the morning sector may be related to a slightly different version of the instability than the one which becomes active at time of the explosive poleward motion. These events may precondition the ionosphere and magnetosphere to allow onset by a different means to take place.

6. Summary and Conclusions

New aspects of the substorm process leading up to the explosive poleward motion of the auroras near substorm onset have been described. Definitions of onset have been compared. AAFs can play an important role in understanding the initial stages of the substorm process and should be taken into account in theories which claim to explain the onset process. A summary of the observations in this paper are listed below:

1. The wavelengths in Earth radii associated with AAFs are greater than $0.05L$. The range in mode number is from about 30 to 135. This result is consistent with the Alfvén-ballooning mode instability and is inconsistent with a cavity mode resonance. This instability may be helped to grow when azimuthal pressure gradients occur in the inner magnetosphere. The AAFs can occur before strong Pi 2 activity and before geosynchronous orbit energetic particle injection. These AAFs can develop into auroral spirals which are wound oppositely to what is expected from the KHI flow vorticity indicating they are associated with magnetic vorticity in an upward field-aligned current sheet. Radar observations of flow surrounding the AAFs confirm this view. They usually occur before the explosive poleward expansion and are sometimes seen along with omega bands. They brighten together with the auroral surge and so can be causally related to the onset mechanism. This result provides definitive proof of a growth phase of an auroral substorm in the ionosphere.

2. The region of brightening prior to poleward expansion is typically 1 hour wide and lies on the main or equatorward UV oval in the case that a double oval configuration exists. This lies 5 to 10 deg equatorward of the region associated with the PSBL and the open-closed field line boundary. About 20% of

the onsets studied in this paper were found to be of this type. They begin in a region which is normally LACPS precipitation but which changes to LABPS at onset. It lies poleward of the energetic IB proton boundaries and the peak in proton precipitation, very close to the energetic (> 100 keV) electron isotropic boundary. A further constraint puts the activations equatorward of where 80 to 250 keV proton precipitation rapidly decreases. This puts the onset earthward of where large pressure gradients begin in the magnetosphere but within the region of nonadiabatic motion of energetic ions. These observations indicate that models involving the PSBL or the open-closed field line boundary as the source region for at least these types of onset are likely to be incorrect. They also indicate that AAFs and omega bands have a near-Earth source region.

3. AAF onsets are sometimes initiated by solar wind pressure changes but this appears to depend somewhat on fluctuations in IMF B_z . They tend to occur when IMF B_z is directed southward. AAF onsets seem to occur preferentially under high solar wind pressure conditions. Coupling via auroral streamers to the high-latitude auroral arc system can sometimes trigger an AAF onset. Thus the PSBL or the open-closed field line boundary may sometimes play an indirect role in substorm onset. In the future, auroral streamer events should be compared with BBF events to determine if a relationship between them exists.

4. AAFs and the associated ground Pc 5 pulsations tend to propagate eastward in the morning and westward in the evening. Azimuthally polarized ground magnetic pulsations in Pc 5 range can be observed before onset. These can gradually change frequency over time and the change can vary with magnetic local time. The frequency of the magnetic pulsations appear to be consistent with the observations of propagation speed and wavelengths of the AAFs.

5. A series of localized activations or pseudobreakups are sometimes followed by a major onset which can occur in a more dipolar tail configuration than existed during the previous activations. Field-aligned currents apparently associated with the substorm current wedge can appear at geosynchronous satellites before the dipolarization effects are observed.

6. Activations which begin from the main UV oval during a double oval configuration take 5 to 10 min to reach near the open-closed field line region. This constrains near-Earth reconnection models such that the last closed field line is not reconnected until this time. It also demonstrates that the substorm bulge should not be identified with the separatrix. This point combined with point 3 indicates that the inner (outer) portion of the magnetosphere can begin a disturbance which propagates tailward (earthward) which eventually affects the outer (inner) magnetosphere.

7. Pseudobreakups characterized as localized intensifications may or may not have associated with them field dipolarizations and energetic particle injections at geosynchronous orbit. It is not clear what governs this relationship. It is clear, however, that the history of a given substorm event is fundamental to understanding it and to placing it in the context of substorm morphology. Without this context, oversimplifications can occur which lead to misunderstandings and disagreements concerning the substorm process. Conflicting views as to the definition and description of an auroral substorm have led us to propose a modular view of the substorm process. This concept allows for a particular substorm to be a composite of one or more modular elements assembled temporally in series or parallel. This change in viewpoint could help resolve inappropriate comparisons being made between various "substorm" events.

Acknowledgments. The authors would like to thank Ann Marie Morris for helping with the manuscript. The Viking project was managed by the Swedish Space Corporation under contract to the Swedish Board for Space Activities. The UV imager was built as a project of the National Research Council of Canada and this work was supported under grants from the Natural Sciences & Engineering Research Council of Canada. The Lockheed portion of this work was supported by NASA contract number NAS5-30565. G. D. Reeves was supported by the U. S. DoE Office of Basic Energy Science. The work of one of the authors was supported by the Russian Foundation of Fundamental Researches grant 93-05-8722. The authors would like to acknowledge F. J. Rich for supplying the DMSP-F7 particle data. The authors thank the referees for the constructive comments.

The Editor thanks A. Otto and T. E. Eastman for their assistance in evaluating this paper.

References

- Akasofu, S.-I., The development of the auroral substorm, *Planet. Space Sci.*, **12**, 273, 1964.
- Akasofu, S.-I., Electrodynamics of the magnetosphere: Geomagnetic storms, *Space Sci. Rev.*, **6**, 21, 1966.
- Akasofu, S.-I., and J. R. Kan, Importance of initial ionospheric conductivity on substorm onset, *Planet. Space Sci.*, **30**, 1315, 1982.
- Akasofu, S.-I., and D. S. Kimball, The dynamics of the aurora, 1. Instabilities of the aurora, *J. Atmos. Phys.*, **26**, 205, 1964.
- Akasofu, S.-I., and A. L. Snyder, Comments on the growth phase of magnetospheric substorms, *J. Geophys. Res.*, **77**, 6275, 1972.
- Anger, C. D., et al., An ultraviolet auroral imager for the Viking spacecraft, *Geophys. Res. Lett.*, **14**, 387, 1987.
- Angelopoulos, V., W. Baumjohann, C. F. Kennel, F. V. Corinitti, M. G. Kivelson, R. Pellat, R. J. Walker, H. Luhr, and G. Paschmann, Bursty bulk flows in the inner central plasma sheet, *J. Geophys. Res.*, **97**, 4027, 1992.
- Atkinson, G., Mechanism by which merging at X lines causes discrete auroral arcs, *J. Geophys. Res.*, **97**, 1337, 1992.
- Baker, D. N., T. I. Pulkkinen, R. L. McPherron, J. D. Craven, L. A. Frank, R. D. Elphinstone, J. S. Murphree, J. F. Fennell, R. E. Lopez, and T. Nagai, CDAW 9 analysis of magnetospheric events on May 3, 1986: Event C, *J. Geophys. Res.*, **98**, 3815, 1993.
- Baumjohann, W., R. J. Pellinen, H. J. Opgenoorth, and E. Nielsen, Joint two-dimensional observations of ground magnetic and ionospheric electric fields associated with auroral zone currents: Current systems associated with local auroral breakups, *Planet. Space Sci.*, **29**, 431, 1981.
- Chan, A. A., M. Xia, L.. Chen, Anisotropic Alfvén-ballooning modes in Earth's Magnetosphere, *J. Geophys. Res.*, **99**, 17,351, 1994.
- Cogger, L. L., and R. D. Elphinstone, The Viking auroral substorm, Proceedings of the First ICS-1, *Eur. Space Agency Spec. Publ.*, **335**, 77, 1992.
- Cogger, L. L., J. S. Murphree, and C. D. Anger, High space and time resolution ultraviolet auroral images from the Viking spacecraft, *Phys. Scr.*, **37**, 432, 1988.
- Elphinstone, R. D., and D. J. Hearn, Mapping of the auroral distribution during quiet times and substorm recovery, Proceedings of the First ICS-1, *Eur. Space Agency Spec. Publ.*, **335**, 13, 1992.
- Elphinstone, R. D., and D. J. Hearn, The auroral distribution and its relation to magnetospheric processes, *Adv. Space Res.*, **13** (4), 17, 1993.
- Elphinstone, R. D., J. S. Murphree, L. L. Cogger, D. Hearn, M. G. Henderson, and R. Lundin, Observations of changes to the auroral distribution prior to substorm onset, in *Magnetospheric Substorms, Geophys. Monogr. Ser.*, vol. 64, edited by J. R. Kan, T. A. Potemra, S. Kokubun, and T. Iijima, p. 257, AGU, Washington, D. C., 1991a.
- Elphinstone, R. D., D. J. Hearn, J. S. Murphree, and L. L. Cogger, Mapping using the Tsyganenko long magnetospheric model and its relationship to Viking auroral images, *J. Geophys. Res.*, **96**, 1467, 1991b.
- Elphinstone, R. D., J. S. Murphree, D. J. Hearn, W. Heikkilä, L. L. Cogger, and I. Sandahl, The auroral distribution and its mapping according to substorm phase, *J. Atmos. Terr. Phys.*, **55** (14), 1741, 1993a.
- Elphinstone, R. D., D. J. Hearn, J. S. Murphree, L. L. Cogger, M. L. Johnson, and H. B. Vo, Some UV dayside auroral morphologies, in *Auroral Plasma Dynamics, Geophys. Monogr. Ser.*, vol. 80, edited by R. L. Lysak, p. 31, AGU, Washington, D. C., 1993b.
- Elphinstone, R. D., D. J. Hearn, L. L. Cogger, I. Sandahl, D. Klumpar, and M. Shapshak, The double oval UV auroral distribution: Implications for the substorm process, paper presented at ICS-2 Proceedings, Fairbanks, Alaska, March 7-11, 1994.
- Erickson, G. M., and M. Heinemann, A mechanism for magnetospheric substorms, Proceedings of the First ICS-1, *Eur. Space Agency Spec. Publ.*, **335**, 587, 1992.
- Fairfield, D. H., Advances in magnetospheric storm and substorm research, *J. Geophys. Res.*, **97**, 10,865, 1992.
- Feldstein, Y. I., Night-time aurora and its relation to the magnetosphere, *Ann. Geophys.*, **30** (2), 259, 1974.
- Feldstein, Y. I., and G. V. Starkov, Dynamics of auroral belt and polar geomagnetic disturbances, *Planet. Space Sci.*, **15**, 209, 1967.
- Goertz, C. K., and R. W. Boswell, Magnetosphere-ionosphere coupling, *J. Geophys. Res.*, **84**, 7239, 1979.
- Goertz, C. K., and R. A. Smith, The thermal catastrophe model of substorms, *J. Geophys. Res.*, **94**, 6581, 1989.
- Haerendel, G., Disruption, Ballooning or auroral avalanche - On the cause of substorms, Proceedings of the First ICS-1, *Eur. Space Agency Spec. Publ.*, **335**, 417, 1992.
- Hallinan, T. J., Auroral spirals, 2, Theory, *J. Geophys. Res.*, **81**, 3959, 1976.
- Hearn, D. J., R. D. Elphinstone, J. S. Murphree, and L. L. Cogger, Geographic asymmetries of the Viking auroral distribution: Implications for ionospheric coordinate systems, *J. Geophys. Res.*, **98**, 1653, 1993.
- Hopcraft, K. I., and P. R. Smith, Polarization characteristics of Pi 2 oscillations, *Planet. Space Sci.*, **34**, 1259, 1986a.
- Hopcraft, K. I., and P. R. Smith, Magnetohydrodynamic waves in a neutral sheet, *Planet. Space Sci.*, **34**, 1253, 1986b.
- Ivanov, V. N., and O. P. Pokhotelov, Flute instability in the plasma shell of the Earth's magnetosphere, *Sov. J. Plasma Phys.*, **13**, 833, 1987.
- Ivanov, V. N., V. A. Marchenko, and O. P. Pokhotelov, The flute instability with unconstant pressure and the qualitative interpretation of the westward travelling surge, *Res. Geomagn. Aeron. Sol. Phys.*, **90**, 52, 1990.
- Ivanov, V. N., O. P. Pokhotelov, F. Z. Feygin, A. Roux, S. Perraut, and D. Leko, Magnetosphere with irregular pressure and a finite beta, *Geomagn. Aeron.*, **32**, 211, 1992.

- Kamide, Y., S.-I. Akasofu, and E. P. Reiger, Co-existence of two substorms in the midnight sector, *J. Geophys. Res.*, **82**, 1620, 1977.
- Kan, J. R., A global magnetosphere-ionosphere coupling model of substorms, *J. Geophys. Res.*, **98**, 17,263, 1993.
- Kennel, C. F., The Kiruna conjecture: The strong version, Proceedings of the First ICS-1, *Eur. Space Agency Spec. Publ.*, **335**, 599, 1992.
- Kirkwood, S., and L. Eliasson, Energetic particle precipitation in the substorm growth phase measured by EISCAT and Viking, *J. Geophys. Res.*, **95**, 6025, 1990.
- Koskinen, H. E. J., R. E. Lopez, R. J. Pellinen, T. I. Pulkkinen, D. N. Baker, and T. Bosinger, Pseudobreakup and substorm growth phase in the ionosphere and magnetosphere, *J. Geophys. Res.*, **98**, 5801, 1993.
- Liu, W. W., and G. Rostoker, On the origin of auroral fingers, *J. Geophys. Res.*, **98**, 17,401, 1993.
- Lui, A. T. Y., A synthesis of magnetospheric substorm models, *J. Geophys. Res.*, **96**, 1849, 1991.
- Lui, A. T. Y., C.-L. Chang, A. Mankofsky, H.-K. Wong, and D. Winske, A cross-field current instability for substorm expansions, *J. Geophys. Res.*, **96**, 11,389, 1991.
- Lui, A. T. Y., R. E. Lopez, B. J. Anderson, K. Takahashi, L. J. Zanetti, R. W. McEntire, T. A. Potemra, D. M. Klumpar, E. M. Greene, and R. Strangeway, Current disruptions in the near-Earth neutral sheet region, *J. Geophys. Res.*, **97**, 1461, 1992.
- Lysak, R. L., J. Grieger, and Y. Song, Fast ionospheric feedback instability and substorm onset, Proceedings of the First ICS-1, *Eur. Space Agency Spec. Publ.*, **335**, 231, 1992.
- Lyons, L. R., Association between tail substorm phenomena and magnetic separation distortion, in *Magnetospheric Substorms*, *Geophys. Monogr. Ser.*, vol. 64, edited by J. R. Kan, T. A. Potemra, S. Kokubun, and T. Iijima, p. 257, AGU, Washington, D. C., 1991.
- McPherron, R. L., Growth phase of magnetospheric substorms, *J. Geophys. Res.*, **75**, 5592, 1970.
- McPherron, R. L., Magnetospheric substorms, *Rev. Geophys.*, **17**, 657, 1979.
- Murphree, J. S., and R. D. Elphinstone, Correlative studies using the Viking imagery, *Adv. Space Res.*, **8**, 9, 1988.
- Murphree, J. S., and L. L. Cogger, The Application of CCD detectors to UV imaging from a spinning satellite, in *Proceedings of SPIE - The International Society for Optical Engineering*, vol. 932, Ultraviolet Technology II, p. 42, 1988.
- Murphree, J. S., and L. L. Cogger, Observations of substorm breakup, in *Proceedings of the First International Conference on Substorms*, pp. 207-211, Eur. Space Agency, Kiruna, Sweden, 1992.
- Murphree, J. S., R. D. Elphinstone, M. G. Henderson, L. L. Cogger, and D. J. Hearn, Interpretation of optical substorm onset observations, *J. Atmos. Terr. Phys.*, **55**, 1159, 1993.
- Murphree, J. S., M. L. Johnson, L. L. Cogger, and D. J. Hearn, Freja UV imager observations of spatially periodic auroral distortions, *Geophys. Res. Lett.*, **21**(17), 1887, 1994.
- Nakamura, R., T. Oguti, T. Yamamoto, and S. Kokubun, Equatorward and poleward expansion of the auroras during auroral substorms, *J. Geophys. Res.*, **98**, 5743, 1993.
- Nakamura, R., D. N. Baker, T. Yamamoto, R. D. Belian, E. A. Bering III, J. R. Benbrook, and J. R. Theall, Particle and field signatures during pseudobreakup and major expansion onset, *J. Geophys. Res.*, **99**, 207, 1994.
- Newell, P. T., S. Wing, C.-I. Meng, and V. Sigillito, The auroral oval position, structure, and intensity of precipitation from 1984 onward: An automated on-line data base, *J. Geophys. Res.*, **96**, 5877, 1991.
- Nielsen, E., The STARE system and some of its applications, in *The IMS Source Book: Guide to the International Magnetospheric Study Analysis*, edited by C. T. Russell and D. J. Southwood, p. 213, AGU, Washington, D. C., 1982.
- Nielsen, E., R. D. Elphinstone, D. J. Hearn, J. S. Murphree, and T. Potemra, Oval intensification event observed by STARE and Viking, *J. Geophys. Res.*, **98**, 6163, 1993.
- Ohtani, S., and T. Tamao, Does the ballooning instability trigger substorms in the near-Earth magnetotail, *J. Geophys. Res.*, **98**, 19,369, 1993.
- Ohtani, S., et al., A multisatellite study of a pseudo-substorm onset in the near-earth magnetotail, *J. Geophys. Res.*, **98**, 19,355, 1993.
- Opgenoorth, H., J. Oksman, K. U. Kaila, E. Nielsen, and W. Baumjohann, On the characteristics of eastward drifting omega bands in the morning sector, *J. Geophys. Res.*, **88**, 9171, 1983.
- Pellinen, R. J., and W. J. Heikkila, Observations of auroral fading before breakup, *J. Geophys. Res.*, **83**, 4207, 1978.
- Pu, Z. Y., A. Korth, and G. Kremser, Plasma and magnetic field parameters at substorm onsets derived from GEOS 2 observations, *J. Geophys. Res.*, **97**, 19,341, 1992.
- Pytte, T., H. Trefall, G. Kremser, L. Jalonen, and W. Riedler, On the morphology of energetic (> 30 KeV) electron precipitation during the growth phase of magnetospheric substorms, *J. Atmos. Terr. Phys.*, **38**, 739, 1976.
- Reeves, G. D., G. Kettmann, T. A. Fritz, and R. D. Belian, Further investigation of the CDAW 7 substorm using geosynchronous particle data: Multiple injections and their implications, *J. Geophys. Res.*, **97**, 6417, 1992.
- Reeves, G. D., T. A. Fritz, R. D. Belian, R. W. McEntire, D. J. Williams, E. C. Roelof, M. G. Kivelson, and B. Wilken, Structured plasma sheet thinning observed by Galileo and 1984-129, *J. Geophys. Res.*, **98**, 21,323, 1993a.
- Reeves, G. D., Multiple substorm injections and the new substorm paradigm: Interpretation of the CDAW 7 substorm, *Adv. Space Res.*, **13**, 213, 1993b.
- Rostoker, G., and T. Eastman, A boundary layer model for magnetospheric substorms, *J. Geophys. Res.*, **92**, 12,187, 1987.
- Roux, A., S. Perraut, P. Robert, A. Morane, A. Pedersen, A. Korth, G. Kremser, B. Aparicio, D. Rodgers, and R. Pellinen, Plasmasheet instability related to the westward travelling surge, *J. Geophys. Res.*, **96**, 17,697, 1991a.
- Roux, A., S. Perraut, A. Morane, P. Robert, A. Korth, G. Kremser, A. Pederson, R. Pellinen, and Z. Y. Pu, Role of the near Earth plasmasheet at substorms, in *Magnetospheric Substorms*, *Geophys. Monogr. Ser.*, vol. 64, edited by J. R. Kan, T. A. Potemra, S. Kokubun, and T. Iijima, p. 201, AGU, Washington, D. C., 1991b.
- Royrvik, O., and T. N. Davis, Pulsating aurora: Local and global morphology, *J. Geophys. Res.*, **82**, 4720, 1977.
- Sergeev, V., E. M. Sazhina, N. A. Tsyganenko, J. A. Lundblad, and F. Soraas, Pitch-angle scattering of energetic protons in the magnetotail current sheet as the dominant source of their isotropic precipitation into the nightside ionosphere, *Planet. Space Sci.*, **31**, 1147, 1983.
- Sergeev, V. A., N. P. Dmitrieva, and E. S. Barkova, Triggering

- of substorm expansion by the IMF directional discontinuities: Time delay analysis, *Planet. Space Sci.*, **34**, 1109, 1986.
- Sergeev, V. A., T. Bosinger, R. D. Belian, G. D. Reeves, and T. E. Cayton, Drifting holes in the energetic electron flux at geosynchronous orbit following substorm onset, *J. Geophys. Res.*, **97**, 6541, 1992.
- Sergeev, V., M. Malkov, and K. Mursula, Testing the isotropic boundary algorithm method to evaluate the magnetic field configuration in the tail, *J. Geophys. Res.*, **98**, 7609, 1993.
- Shepherd, G. G., and J. S. Murphree, Diagnosis of auroral dynamics using global auroral imaging with emphasis on localized and transient features, *Proceedings of the International Conference on Auroral Physics*, pp. 289-297, Cambridge University Press, New York, 1988.
- Singer, H. J., W. J. Hughes, C. Gelpi, and B. G. Ledley, Magnetic disturbances in the vicinity of synchronous orbit and the substorm current wedge: A case study, *J. Geophys. Res.*, **90**, 9583, 1985.
- Starkov, G. V., and Y. I. Feldstein, Auroral substorm, *Geomagn. Aeron.*, **11**, 560, 1971.
- Swift, D. W., The possible relationship between the auroral breakup and the interchange instability of the ring current, *Planet. Space Sci.*, **15**, 1225, 1967.
- Takahashi, K., R. Lopez, R. W. McEntire, L. J. Zanetti, L. M. Kistler, and F. M. Ipavich, An eastward propagating compressional Pc 5 wave observed by Ampte/CCE in the postmidnight sector, *J. Geophys. Res.*, **92**, 13,472, 1987.
- Thomas, R. W., and M. C. Stenbaek-Nielsen, Recurrent propagating auroral forms in pulsating aurora, *J. Atmos. Terr. Phys.*, **43**, 243, 1981.
- Tsyganenko, N. A., Global quantitative models of the geomagnetic field in the cislunar magnetosphere for different disturbance levels, *Planet. Space Sci.*, **35**, 1347, 1987.
- Tsyganenko, N. A., A magnetospheric magnetic field model with a warped tail current sheet, *Planet. Space Sci.*, **37**, 5, 1989.
- Ullaland, S., G. Kremser, P. Tanskanen, A. Korth, A. Roux, K. Torkar, L. P. Block, and I. B. Iversen, On the development of a magnetospheric substorm influenced by a storm sudden commencement: Ground, balloon, and satellite observations, *J. Geophys. Res.*, **98**, 15,381, 1993.
- Untiedt, J., R. Pellinen, F. Kuppers, H. J. Opgenoorth, W. D. Pelster, W. Baumjohann, H. Ranta, J. Kangas, P. Czechowsky, W. J. Heikkila, Observations of the initial development of an auroral and magnetic substorm at magnetic midnight, *J. Geophys.*, **45**, 41, 1978.
- Vetoulis, G. and L. Chen, Global structures of Alfvén-ballooning modes in magnetospheric plasmas, *Geophys. Res. Lett.*, **21**(19), 2091, 1994.
- Watanabe, M., and T. Iijima, Substorm growth phase on the magnetotail, *J. Geophys. Res.*, **98**, 17,299, 1993.
- Yahnin, A. G., T. Bosinger, J. Kangas, and R. D. Belian, Some implications of multiple peak structure of drifting high energy proton clouds for substorm dynamics as inferred from ground satellite correlations, *Ann. Geophys.*, **8**, 327, 1990.
- Zelenyi, L. M., R. A. Kovrazhkin, and J. M. Bosqued, Velocity dispersed ion beams in the nightside auroral zone: Aureol 3 observations, *J. Geophys. Res.*, **95**, 12,119, 1990.
-
- L. L. Cogger, R. D. Elphinstone, D. J. Hearn, M. Johnson, and J. S. Murphree, Department of Physics and Astronomy, University of Calgary, Calgary, Alberta T2N 1N4, Canada.
- Y. I. Feldstein, IZMIRAN, Moscow Region, Troitsk 142092, Russia.
- D. M. Klumpar, Space Science Laboratory, Lockheed Missiles and Space Co. Inc., Palo Alto, CA 94304-1911.
- K. Mursula, Department of Physics, University of Oulu, Oulu, Finland SF 90570.
- P. T. Newell, S. Ohtani, and T. A. Potemra, Applied Physics Laboratory, Johns Hopkins University, Laurel, MD 20723.
- E. Nielsen, Max-Planck-Institute for Aeronomy, Lindau D-3411, Germany.
- H. Opgenoorth and M. Persson, Swedish Institute for Space Physics, Uppsala S-755-90, Sweden.
- G. D. Reeves, Los Alamos National Laboratory, Los Alamos, NM 87545.
- I. Sandahl, Swedish Institute for Space Physics, Kiruna, S-981-28, Sweden.
- V. Sergeev, Institute of Physics, University of St. Petersburg, St. Petersburg, Russia.
- H. Singer, NOAA R/E/SE, 325 Broadway, Boulder, CO 80303-3328.

(Received June 16, 1994; revised October 18, 1994; accepted November 9, 1994.)